

431.5
Y66
(H0)

アゾベンゼン高分子を用いたホログラム記録法の実用化研究

課題番号：13555009

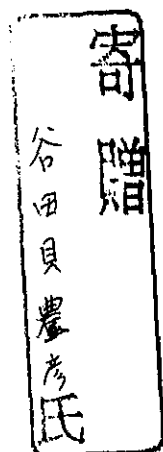
平成13年度～平成14年度科学研究費補助金

基盤研究（B）（2）研究成果報告書

平成15年3月

研究代表者 谷田貝 豊彦

（筑波大学物理工学系教授）



03601434

平成13年度～平成14年度科学研究費補助金
基盤研究（B）（2）研究成果報告書

I. 研究課題と研究組織

1. 研究課題： アゾベンゼン高分子を用いたホログラム記録法の実用化研究

2. 課題番号： 13555009

1. 研究組織

研究代表者： 谷田貝 豊彦 筑波大学物理工学系 教授

研究分担者： 伊藤 雅英 筑波大学物理工学系 助教授

原田 建治 筑波大学物理工学系 講師（平成14年3月まで）

2. 研究費

交付決定額（配分額） (金額単位：千円)

	直接経費	間接経費	合計
平成13年度	8,500	0	8,500
平成14年度	3,900	0	3,900
総計	12,400	0	12,400

II. 研究発表

論文

1. A new holographic recording material and its diffraction efficiency increase effect: the use of photoinduced surface deformation in azo-polymer film, Katsuhiro Munakata, Kenji Harada, Masahide Itoh, Shinsuke Umegaki, Toyohiko Yatagai, Optics Communications, **191**, 15-19(2001).
2. Diffraction efficiency increase by corona discharge in photoinduced surface-relief gratings on an azo polymer film, K. Munakata, K. Harada, H. Anji, M. Itoh, T. Yatagai and S. Umegaki, Opt. Lett., **26**, 4-6(2001).
3. Retardation modulated differential interference microscope and its application for phase analysis, Toyohiko Yatagai, Masahide Itoh, Hiroto Nozawa and Hiroshi Ishiwata, Fringe 2001(The 4 th International Workshop on Automatic Processing of Fringe Patterns),181-186(2001).
4. Analysis of spatiotemporal coupling in a femtosecond pulse shaper by the Wigner distribution function, Yasunori Sutoh, Yoshiaki Yasuno, Kenji Harada, Masahide Itoh, Masahiko Mori and Toyohiko Yatagai, Opt. Eng., **40**, 1717-1723(2001).
5. Holographic Recording and Control of Diffraction Efficiency Using Photoinduced Surface Deformation on Azo-Polymer Films, K. Harada, H. Inoue, M. A. El-Morsy. M. Itoh, S. Umegaki and T. Yatagai, Jpn. J. Appl. Phys., **41**, 1851-1854(2002).
6. Surface Relief Holograms on azo-polymer film Toyohiko Yatagai and Kenji Harada, Technical Program and Summary Digest (2002 International Meeting on Information Display), 293-296(2002),
7. Multiple-Beam Fizeau Fringe-Pattern Analysis Using Fourier Transform Method for Accurate Measurement of Fiber Refractive Index Profile of Polymer Fiber, M. A. El-Morsy, Y. Yatagai, A. Hamza, M. A. Mabrouk and T. Z. N. Sokkar, Journal of Applied Polymer Science, **85**, 475-484(2002).
8. Automatic refractive index profiling of fibers by phase analysis method using Fourier transform , M. A. El-Morsy, T. Yatagai, A. A. Hamaza, M. A. Mabrouk, and T. Z. N. Sokkar , Optics and Lasers in Engineering , **38**, 509-525(2002).
9. Spatial light manipulation devices using nonlinear polymeric materials, K. Harada, K. Munakata, M. Itoh, S. Umegaki and T. Yatagai, Optical and Quantum Electronics, **34**, 1183-1189(2002).
10. A subfringe integration method for multiple-beam Fizeau fringe analysis, M. A. El-Morsy, K. Harada, M. Itoh and T. Yatagai, Optics & Laser Technology, **35**, 223-232(2003).

口頭発表

1. 分子シンクロナイゼーション光デバイス
谷田貝豊彦
第48回応用物理学関係連合講演会 明治大学
2001年3月28日-31日
2. アゾベンゼン高分子薄膜を用いたホログラム記録
宗形勝博、原田建治、井上大、伊藤雅英、梅垣真祐、谷田貝豊彦
第48回応用物理学関係連合講演会 明治大学 2001/3/28-31
3. コロナ帯電による表面レリーフグレーティングの特性変化とその応用
井上大、宗形勝博、原田建治、伊藤雅英、梅垣真祐、谷田貝豊彦
第48回応用物理学関係連合講演会 明治大学 2001/3/28-31
4. 立体動画像表示と空間光変調器
谷田貝豊彦
高分子エレクトロニクス研究会 上智大学中央図書館棟 2001/5/11
5. Retardation modulated differential interference microscope and its application for phase analysis
T. Yatagai, M. Itoh, H. Nozawa and H. Ishiwata
FRINGE 2001 (The 4th International Workshop on Automatic Processing of Fringe Patterns) Bremen, Germany 2001/9/17-19
6. Direct fabrication method of surface relief structures on azo-polymer films and its device application
K. Harada, M. Itoh, S. Umegaki and T. Yatagai
International Forum on Nanotechnology : Toward the Organic Photonics (2nd Chitose International Forum on Photonics Science & Technology) 千歳科学技術大学(北海道) 2001/9/6-8
7. アシスト光照射によるアゾベンゼン高分子薄膜上への表面レリーフホログラム記録
原田建治, 井上大, 伊藤雅英, 梅垣真祐, 谷田貝豊彦
第62回秋季応用物理学会学術講演会
愛知工業大学 2001/9/11-14
8. 2次非線形高分子材料を用いた光変調デバイス
(Light modulator using second-order nonlinear photopolymer)
谷田貝豊彦, 原田建治
第81回微小光学研究会 「有機微小光学」 横浜, 東工大 2001/9/5
9. Photoinduced surface deformation on azo-polymer films and its device applications
Toyohiko Yatagai and Kenji Harada

Fourth Japan-Finland Joint Symposium on OPTICS IN ENGINEERING (OIE '01)
Osaka University, Osaka 2001/10/25-27

- 1 0. Holographic recordings of surface relief structures on azo-polymer films and its device applications
Kenji Harada, Hajime Inoue, Katsuhiko Munakata, Masahide Itoh, Shinsuke Umegaki and Toyohiko Yatagai
OSA Annual Meeting and Exhibit 2001 • ILS-XVII: 17th Interdisciplinary Laser Science Conference Long Beach, California, USA 2001/10/14-18
- 1 1. Holographic recording on azo-polymer film K.
Harada and Y. Yatagai
Electronic Imaging 2002 Science and Technology (IS&T/SPIE's 14th Annual Symposium) San Jose, California USA 2002/1/20-25
- 1 2. 偏光感受型スペクトル干渉光コヒーレンストモグラフィ
安野嘉晃、須藤泰範、巻田修一、伊藤雅英、谷田貝豊彦
第49回応用物理学関係連合講演会 東海大学 2002/3/27-30
- 1 3. コロナ帯電を利用した光誘起表面レリーフ形成とその回折効率制御
原田建治、井上大、伊藤雅英、梅垣真祐、
谷田貝豊彦 第49回応用物理学関係連合講演会 東海大学
2002/3/27-30
- 1 4. Surface Relief Holograms on azo-polymer film
Toyohiko Yatagai and Kenji Harada
2002 International Meeting on Information Display Daegu, Korea
2002/8/21-23
- 1 5. Analysis of near field characteristics of a diffractive optical laser beam profile shaper using a high accuracy finite difference time domain method
S. Banerjee and T. Yatagai
2002 International Optical Design Conference Tucson, Arizona, U. S. A.
2002/6/3-5
- 1 6. Spectral interferometric optical coherence tomography
T. Yatagai
2002 International Conference on Applications of Photonic Technology (Photonics North) Quebec, Canada 2002/6/2-6
- 1 7. アゾベンゼン高分子薄膜を用いた可逆表面レリーフホログラム
原田建治、亀丸俊一、井上大、伊藤雅英、谷田貝豊彦
第63回応用物理学会学術講演会 新潟大学 2002/9/24-27
- 1 8. Measurements of Small Steps by Retardation Modulated Differential Interference Contrast Microscope III (The Analysis of the Rotational Error of the Specimen) 近藤清志、石渡裕、伊藤雅英、谷田貝豊彦

- 日本光学会年次学術講演会 (Optics Japan 2002) 東京農工大 2002/11/2-4
19. Recording of rewritable surface relief hologram on azo-polymer films. Kenji Harada, Hajime Inoue, Masahide Itoh and Toyohiko Yatagai
The 16th Symposium on Optical and Electrical Properties of Organic Materials
2002/5/22-24
20. Surface Relief DOE with Azo-Polymer Film
Toyohiko Yatagai and Kenji Harada
CLEO Europe, Scottish Exhibition & Conference Centre Glasgow, Scotland
2002/11/10-14
21. アゾベンゼン高分子薄膜を用いた表面レリーフ型ホログラム記録
原田建治、井上大、伊藤雅英、梅垣真祐、谷田貝豊彦
平成14年度第1回ホログラフィック・ディスプレイ研究会
印刷博物館 2002/5/31

工業所有権

特許権出願： 井出陽一郎、高橋源昭、原田建治、谷田貝豊彦：
光学材料およびそれを用いた表示装置
特願2002-335427

III. 研究成果

1. はじめに

有機非線形光学材料は一般に非線形感受率が大きく、高速応答が可能である。さらに分子、結晶レベルでの設計、合成が可能であり、光情報処理の様々な分野での応用が期待されている。その中で、アゾベンゼン高分子は吸収波長の光を照射することで分子がトランス体からシス体への異性化する代表的な材料である。光異性化により吸光度や屈折率が変化するため、光記録材料として注目されている。特にアゾ基を側鎖に持つポリマーは、吸収波長のレーザー光を照射することにより表面レリーフグレーティングが簡単に作製できることが知られており、そのメカニズム解明や、ホログラム記録材料としての応用が期待されている。この表面レリーフグレーティングはサンプルをガラス転移温度付近に加熱することにより消去することができる。また、表面レリーフグレーティングに加熱しながらコロナ帯電させることで、逆にレリーフの深さを増大することができる。これを利用することにより、回折効率を自由に制御できる全く新しい可逆ホログラム記録材料としての応用が検討される。アゾベンゼン高分子材料を用いた表面レリーフ型のホログラムの作製や、回折効率の制御についての現在までの研究成果を報告する。

2. アゾベンゼン高分子薄膜の作製

ホログラム記録材料として側鎖型のアゾベンゼン高分子薄膜である Poly-orange Tom-1 Isophoronediiisocyanate を用いた。ガラス転移温度 (T_g) は 136°C である。図1に化学構造及び吸光度を示す。

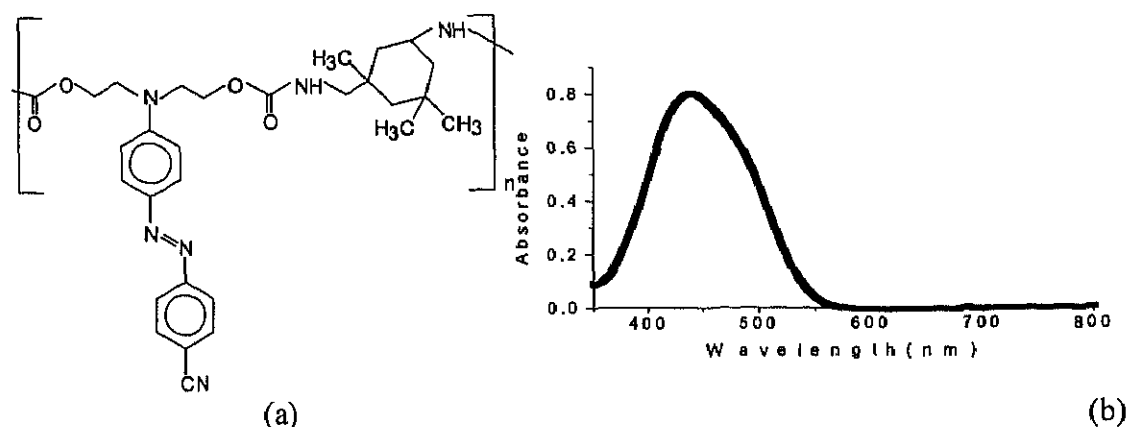


図1 Poly-orange Tom-1 Isophoronediiisocyanate の (a)化学構造および (b)吸光度

溶媒にシクロヘキサノンを用い、超音波槽で30分程度溶解後に $0.5\mu\text{m}$ のフィルターを通した。その溶液をパイレックスガラス上にスピコートすることで、膜厚 $1\mu\text{m}$ 程度に薄膜化した。

3. 表面レリーフグレーティングの作製

図2に示す光学系を用いて表面レリーフグレーティングを作製した。光源には波長488nmの Ar^+ レーザーを用いた。レーザー光は直径6mmにコリメートされ、反射ミラーを用いてサンプル上で2光束を干渉させている。サンプルとミラー間の角度は90度に固定し、サンプルの傾き θ を変えることでグレーティング周期を調整できる。

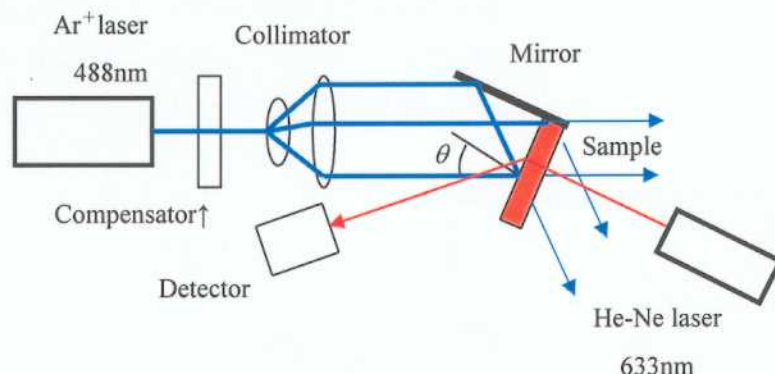


図2 表面レリーフグレーティング作製用光学系

図3にレーザー光強度 $50\text{mW}/\text{cm}^2$ の干渉光を照射したときの表面レリーフグレーティングの1次回折効率の変化を示す。1次回折光強度の測定には、材料の吸収がほとんどないHe-Neレーザー(633nm)を用いた。書き込み偏光を円偏光、p偏光及びs偏光として測定した。円偏光を用いた場合に最も大きな回折効率を得られ、s偏光を入射した際はほとんど変化が見られなかった。作製過程はレーザーの照射エネルギーにも

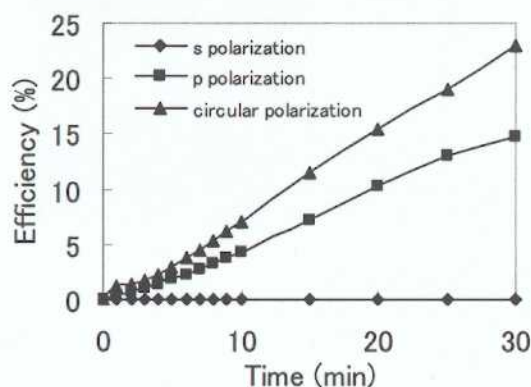


図3 1次回折効率の書き込み偏光依存性

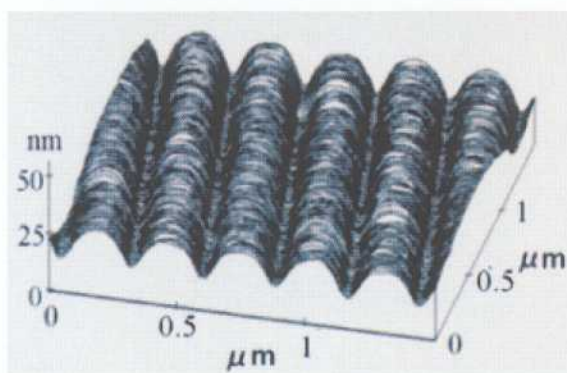


図4 表面レリーフグレーティングのAFM像

依存しており、強い照射強度で書込めば短時間で高い回折効率を得られる。作製した表面レリーフグレーティングのAFM像を図4に示す。最小で、グレーティング間隔275nmのレリーフが作製できた。

4. コロナ帯電による回折効率制御

作製した表面レリーフ構造は、均一光照射や高温下で消去可能であるが、コロナ帯

電を利用することにより逆に増強することができる。コロナ帯電の装置を図5に示す。ガラス転移温度付近で高電圧を印加することにより、フィルム上に電荷が帯電する。通常これによって分子が配向され2次の非線形性が発現する(コロナポーリング)。さらに表面にレリーフ構造があるときは、帯電した電荷によるクーロン力の差により高分子の移動がおこりレリーフ深さが増加する。図6にコロナ帯電前とコロナ帯電後の表面レリーフの変化を示す。レリーフ作製条件はレーザー光強度 $50\text{mW}/\text{cm}^2$ で10分、コロナ帯電条件は 8 kV の印加電圧で20分間とした。

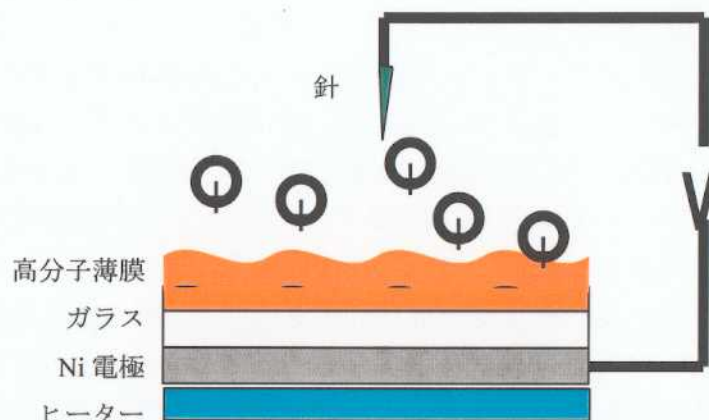


図5 コロナ帯電装置

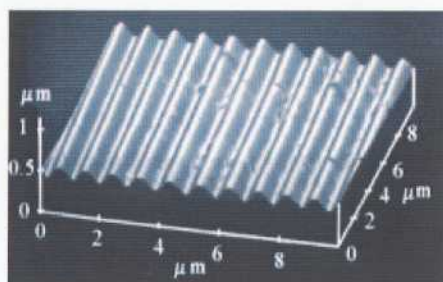
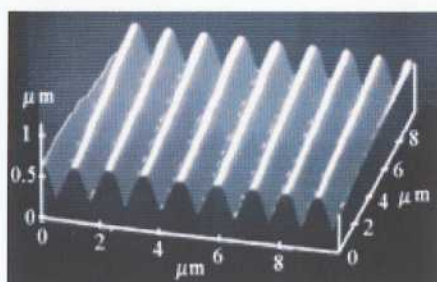


図6(a) コロナ帯電前の AFM 像
(レリーフ深さ 130 nm)



(b) コロナ帯電後の AFM 像
(レリーフ深さ 450 nm)

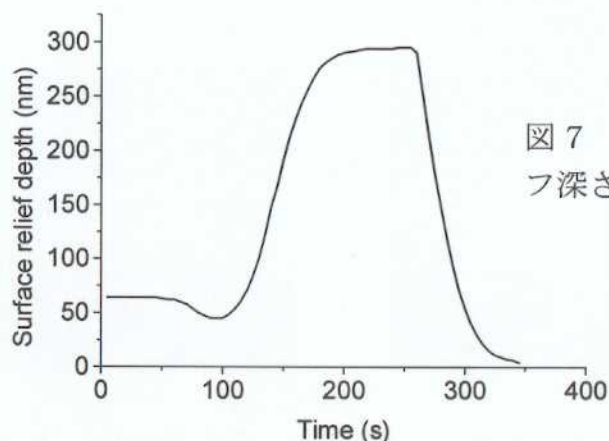


図7 コロナ帯電による表面レリーフ深さの変化

(コロナ帯電条件

・60 秒～260 秒 : 140°C 、 6.5 kV ,

コロナ帯電前のレリーフ深さは 130 nm であったが、帯電により 450 nm に増加した。コロナ帯電時の反射の 1 次回折光を測定することで、コロナ帯電による表面レリーフ深さの変化を計算した。レリーフ作製条件は 220 mW/cm^2 で 30 秒、コロナ帯電電圧は 6.5kV とした。作製したサンプルを 60 秒後に加熱と同時にコロナ帯電した。レリーフ深さはいったん減少するが、すぐに増加しやがて 300 nm 付近で安定する。260 秒後にコロナ帯電の電圧を 0 にすると、レリーフ深さは急激に減少し消去される。このようにコロナ帯電により、自由にレリーフ深さを制御することができる。

5. 表面レリーフホログラム記録

次に、フーリエ変換型およびフレネル型ホログラムを記録した。入力画像としてサイズ $3 \text{ mm} \times 4 \text{ mm}$ の文字 A を用いた (図 8(a))。それをフーリエ変換し、サンプル上で参照光と干渉させることで記録した。記録光強度は 100 mW/cm^2 程度、記録時間は 1 分とした。図 8(b)(c) にフーリエ面での写真および He-Ne レーザーによる再生像を示す。記録時間を 10 分とすると、フーリエ面の中央がブリーチされ、エッジ強調された像が再生された (図 8(d))。また、記録時間 1 分のサンプルをコロナ帯電することにより回折効率が 0.24% から 28% まで増大した (図 8(e))。また、フレネルホログラムについても同様に記録した。記録物体として長さ 3 cm の将棋の駒を使用した。まず歩兵の駒を 20 mW、15 分で記録し再生した (図 9(a))。その後ガラス転移温度で 30 秒加熱して消去後、他の駒の記録、再生、消去を繰り返し、王将の駒を記録、再生した (図 9(b))。繰り返し記録後も良好な再生像が得られた。

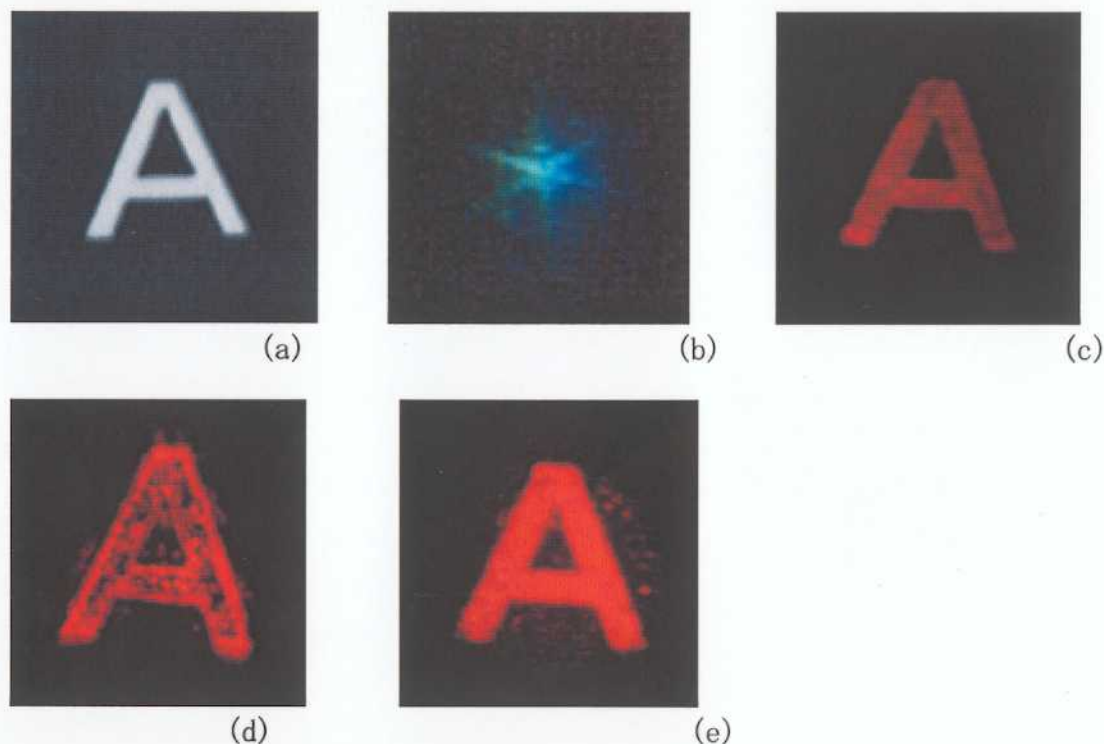
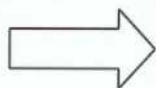


図 8 (a)入力画像 (b)フーリエ面の写真 (c)再生像(記録時間 1 分) (d) 再生像(記録時間 10 分) (e)再生像(記録時間 1 分、コロナ帯電後)



図9 (a) ホログラム再生像
(繰り返し記録回数 1 回)
記録時間 15 分



(b) ホログラム再生像
(繰り返し記録回数 4 回)
記録時間 30 分

6. 結論

アゾベンゼン高分子の光照射による表面レリーフ形成を利用して、フーリエ変換型およびフレネル型ホログラムの記録をした。ガラス転移温度付近への加熱によりレリーフを消去でき、またコロナ帯電を利用することによりレリーフ深さを増加できる。コロナ帯電の電圧調整や、均一光照射により回折効率を制御できることから、今までにない新しいホログラム記録材料としての応用が期待される。

ABSTRACTS OF RESEARCH PROJECT, GRANT-IN-AID
FOR SCIENTIFIC RESEARCH (2002)

1. RESEARCH INSTITUTE NUMBER: 12102
2. RESEARCH INSTITUTION: University of Tsukuba
3. CATEGORY: B
4. TERM OF PROJECT (2001 -2002)
5. PROJECT NUMBER: 13555009
6. TITLE OF PROJECT: Holographic recording using azo-polymers
7. HEAD INVESTIGATOR 90087445 Toyohiko Yatagai, University of Tsukuba,
Institute of Applied Physics, Professor
8. INVESTIGATOR (1) 30150874 Masahide Itoh, University of Tsukuba,
Institute of Applied Physics, Associate Professor
(2) 30312820 Kenji Harada, University of Tsukuba,
Institute of Applied Physics, Assistant Professor

9. SUMMARY OF RESEACH RESULTS

Polymeric materials are the most promising organic materials for electro-optic, and memory devices. In the past several years, direct fabrication of relief structures in azo-polymers has been reported. This method is a one-step fabrication technique. A surface relief structure is fabricated by means of irradiation of interference fringes. We propose a new reversible surface relief hologram using photoinduced surface deformation on azo-polymer films. The diffraction efficiency of the hologram is dramatically increased by corona charging, and it is controlled by applied voltage of the corona charging.

The side-chain azo-polymer, poly-orange tom-1 isophoronedisocyanate, is used in this study. Figure 1 shows the chemical structure the material. The glass transition temperature T_g is 136°C. The absorption peak and the cut-off wavelength of the dye are 440 nm and 560 nm, respectively. This polymer is dissolved in cyclohexanone. Samples of 1~5 μ m thickness are prepared by spin-coating on a slide glass plate. The refractive index of the film is measured as 1.65 at a wavelength of 633 nm by the m-line technique. The surface relief grating is fabricated by the irradiation of two-beam interference fringes.

The mechanism of increasing the diffraction efficiency and the relief depth of a surface relief structure by corona charging at temperatures near or above its T_g is not clearly understood, but we consider that the relief depth increases as a result of the Coulomb force exerted by electric charge; therefore the diffraction efficiency is increased. In the corona charging process, the voltage was applied at a temperature near T_g and the polymer film was heated to the corona charging temperature with the voltage applied, because the surface relief structure is thermally erased above T_g without the applied voltage.

10. KEY WORDS

- (1) Holography, (2) Surface relief grating, (3) Electronic-Field Induced Poled Polymer,
(4) Diffraction optical element,

REFERENCES

AUTHORS, TITLE OF ARTICLE	JOURNAL, VOLUME-NUMBER, PAGES CONCERNED, YEAR
1. A new holographic recording material and its diffraction efficiency increase effect: the use of photoinduced surface deformation in azo-polymer film, Katsuhiko Munakata, Kenji Harada, Masahide Itoh, Shinsuke Umegaki, Toyohiko Yatagai,	Optics Communications, 191 , 15-19(2001).
2. Diffraction efficiency increase by corona discharge in photoinduced surface-relief gratings on an azo polymer film, K. Munakata, K. Harada, H. Anji, M. Itoh, T. Yatagai and S. Umegaki,	Opt. Lett., 26 , 4-6(2001)
3. Retardation modulated differential interference microscope and its application for phase analysis, Toyohiko Yatagai, Masahide Itoh, Hiroto Nozawa and Hiroshi Ishiwata,	Fringe 2001(The 4 th International Workshop on Automatic Processing of Fringe Patterns) 181-186(2001).
4. Analysis of spatiotemporal coupling in a femtosecond pulse shaper by the Wigner distribution function, Yasunori Sutoh, Yoshiaki Yasuno, Kenji Harada, Masahide Itoh, Masahiko Mori and Toyohiko Yatagai,	Opt. Eng. , 40 , 1717-1723(2001).
5. Holographic Recording and Control of Diffraction Efficiency Using Photoinduced Surface Deformation on Azo-Polymer Films, K. Harada, H. Inoue, M. A. El-Morsy, M. Itoh, S. Umegaki and T. Yatagai,	Jpn. J. Appl. Phys., 41 , 1851-1854(2002).
6. Surface Relief Holograms on azo-polymer film Toyohiko Yatagai and Kenji Harada	Technical Program and Summary Digest (2002 International Meeting on Information Display), 293-296(2002), Journal of Applied Polymer Science, 85 , 475-484(2002).
7. Multiple-Beam Fizeau Fringe-Pattern Analysis Using Fourier Transform Method for Accurate Measurement of Fiber Refractive Index Profile of Polymer Fiber, M. A. El-Morsy, Y. Yatagai, A. Hamza, M. A. Mabrouk and T. Z. N. Sokkar,	Optics and Lasers in Engineering , 38 , 509-525(2002).
8. Automatic refractive index profiling of fibers by phase analysis method using Fourier transform , M. A. El-Morsy, T. Yatagai, A. A. Hamaza, M. A. Mabrouk, and T. Z. N. Sokkar ,	Optical and Quantum Electronics, 34 , 1183-1189(2002).
9. Spatial light manipulation devices using nonlinear polymeric materials , K. Harada, K. Munakata, M. Itoh, S. Umegaki and T. Yatagai,	Optics & Laser Technology, 35 , 223-232(2003)
10. A subfringe integration method for multiple-beam Fizeau fringe analysis, M. A. El-Morsy, K. Harada, M. Itoh and T. Yatagai ,	



ELSEVIER

1 May 2001

OPTICS
COMMUNICATIONS

Optics Communications 191 (2001) 15–19

www.elsevier.com/locate/optcom

A new holographic recording material and its diffraction efficiency increase effect: the use of photoinduced surface deformation in azo-polymer film

Katsuhiro Munakata ^{a,*}, Kenji Harada ^a, Masahide Itoh ^a, Shinsuke Umegaki ^b,
Toyohiko Yatagai ^a

^a Institute of Applied Physics, University of Tsukuba, Tennodai 1-1-1, Tsukuba, Ibaraki 305-8573, Japan

^b Faculty of Science and Technology, Keio University, Hiyoshi 3-14-1, Kohoku, Yokohama, Kanagawa 223-0061, Japan

Received 10 November 2000; received in revised form 19 January 2001; accepted 26 January 2001

Abstract

Holographic recording characteristics using a photoinduced surface deformation in a side-chain type azo-polymer film were investigated. Corona charging at temperatures above the glass transition temperature increased the diffraction efficiency of the recorded hologram from 0.24% to about 30% and the relief depth from 20 to 350 nm. © 2001 Elsevier Science B.V. All rights reserved.

Keywords: Hologram; Photoinduced surface deformation; Surface relief grating; Corona discharging; Increase effect

1. Introduction

The most important characteristics of holographic recording material are sensitivity, resolution, maximum diffraction efficiency, and signal-to-noise ratio. Up to now, silver halide has been most commonly used due to its high sensitivity and high resolution. However, photorefractive crystals [1] and photopolymers [2] are also to record a holographic grating after a shorter irradiation time by use of a high power laser beam. These materials show the advantages over silver halide of high resolution and real-time recording.

The recording of polarization holographic gratings using azobenzene-containing polymer films as photoanisotropic materials has been reported [3]. This photoinduced anisotropic effect is due to *trans-cis-trans* isomerization and the orientational effects of the azo-dye chromophore. To record a polarization holographic grating, a setup comprising two mutually orthogonal linear polarization beams and a relatively thick film of over 10 μm is necessary. On the other hand, the direct recording method of a surface relief grating (SRG) on azo polymers has been reported [4–7] in which the grating is recorded by means of a spatially varying intensity distribution combined with a spatially varying polarization distribution [8]. The recording mechanism of this SRG is due to the photoisomerization and the movement of the polymer chains [9,10]. A surface relief type hologram

* Corresponding author. Fax: +81-298-53-5205.

E-mail address: munakata@optlab2.bk.tsukuba.ac.jp (K. Munakata).

can be recorded using this SRG recording technique. The diffraction efficiency of this type of hologram depends on the recording polarization state and the recording energy. This hologram has advantages including real time recording, multiplex recording [11], repetition recording and high diffraction efficiency [4], but the material requires a long recording time to obtain a high diffraction efficiency. We have recently reported that the diffraction efficiency and relief depth of the SRG can be dramatically increased by corona charging at temperatures above the glass transition temperature (T_g) [12]. This process is same as the development process. Using this increase effect by corona charging after the hologram recording by SRG recording technique, the hologram with high diffraction efficiency can be recorded and the recording time can be short, and the diffraction efficiency of the hologram can also be control by the corona charging condition. Still more, this increased hologram has the nonlinearity [13], because the orientation of the azo chromophore and the increasing of the diffraction efficiency are performed concurrently by corona charging.

In this letter, we report Fourier transform hologram recording using a photoinduced surface deformation technique. We also propose a method for increasing the diffraction efficiency of the recorded Fourier transform hologram by means of corona charging.

2. Recording of the surface relief grating

An azo-polymer film was prepared by spin-coating poly-orange tom-1 Isophronediisocyanate [7] on a pyrex glass substrate. The concentration of dye is 18 wt.% and T_g is 136°C. This film has a light absorption peak at the wavelength of 440 nm.

We first measured the recording time dependence of the diffraction efficiency in a SRG recorded using a two-beam interference fringe. A circularly polarized Ar-ion laser beam with a wavelength of 488 nm was used as the light source. We monitored the first-order diffraction efficiency of the SRG using the He-Ne laser beam during the recording. The recording time dependence of the first-order diffraction efficiency is shown in Fig. 1.

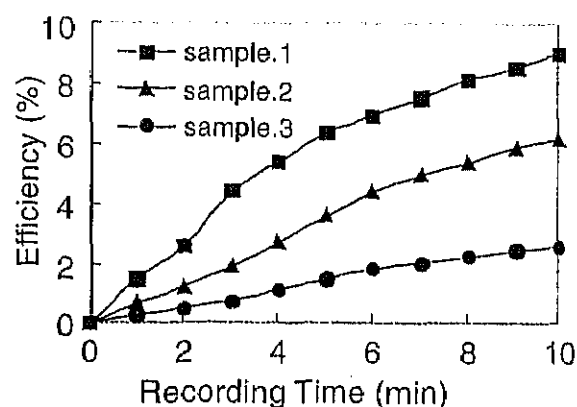


Fig. 1. Time dependence of the first-order diffraction efficiency on the SRG.

The SRGs were recorded in all three cases. The power of two beams are same. The recording power and film thickness were 88 mW/cm² and 2 μ m in Sample 1; 193 mW/cm² and 1 μ m in Sample 2; and 88 mW/cm² and 1 μ m in Sample 3, respectively. The angle between the two beams was set at 30°, resulting in a grating period of about 1 μ m. The diffraction efficiency after 10 min of recording was 9.9% in Sample 1, 6.4% in Sample 2 and 2.6% in Sample 3, respectively. This shows that the diffraction efficiency is dependent on the film thickness and the recording power and time (energy). The high diffraction efficiency can be obtained at a short time by high power recording.

3. Hologram recording and diffraction efficiency increase

3.1. Recording of the Fourier transform hologram

Next, we examined Fourier transform hologram recording using the photoinduced surface modulation technique. The hologram recording setup is shown in Fig. 2. A circularly polarized Ar-ion laser beam with a wavelength of 488 nm was used. The laser beam was collimated with a 6 mm diameter and separated by a beam splitter. The Fourier transform hologram was recorded on the azo-polymer film at a thickness of about 2 μ m as shown in Fig. 3(a) and (b). The letters A and E, each 4 mm tall and 3 mm wide, were used as ob-

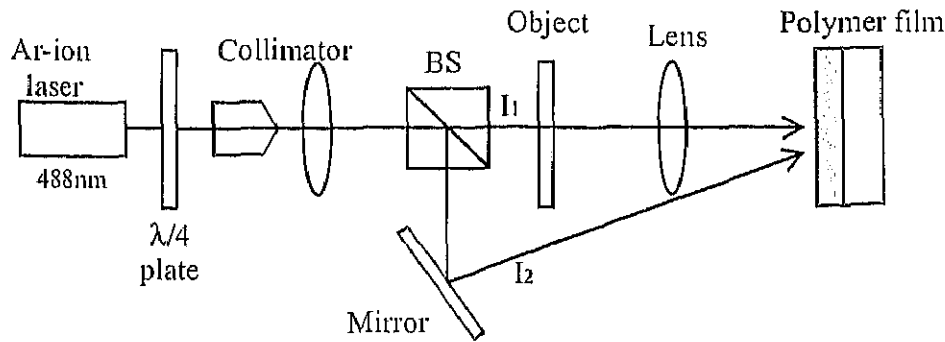


Fig. 2. Experimental setup for the Fourier transform hologram recording.

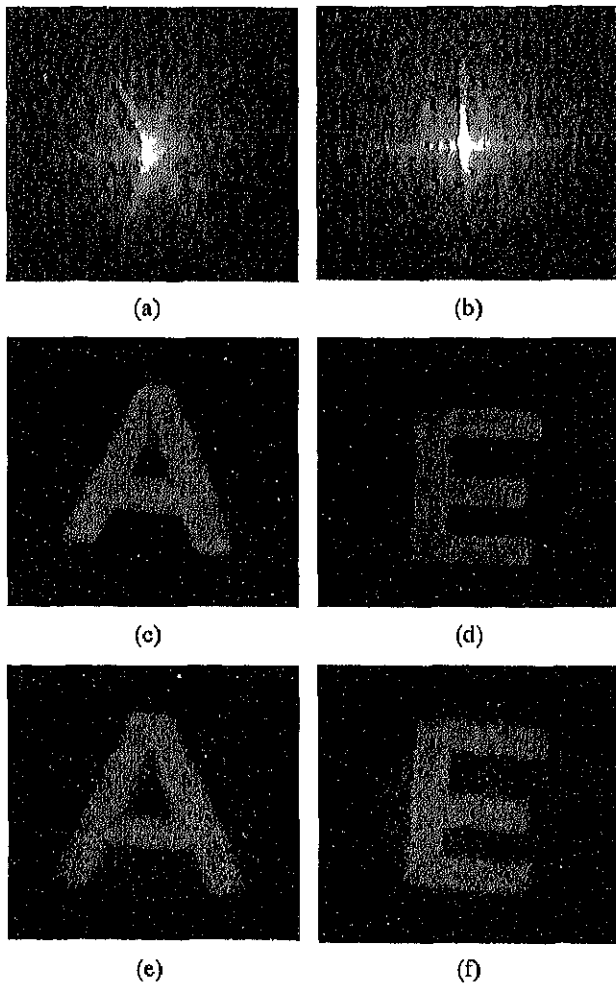


Fig. 3. The Fourier transform holograms of (a) letter A and (b) letter E recorded on the azo-polymer film and the reconstructed images before corona charging of (c) letter A and (d) letter E. The reconstructed images after corona charging of (e) letter A and (f) letter E.

jects. The beam power in front of the object was $I_1 = 118 \text{ mW/cm}^2$. The object beam was Fourier transformed on the azo-polymer film using a lens with a focal length of 100 mm. The reference beam power was $I_2 = 118 \text{ mW/cm}^2$ and the recording time was 1 min. The reconstructed images are shown in Fig. 3(c) and (d). These reconstructed images were observed using a He–Ne laser beam. The diffraction efficiency of the recorded holograms (letters A and E) measured by He–Ne laser beam with 1 mm diameter was about 1.2% and 1%, respectively.

3.2. Diffraction efficiency increase of the hologram

We have recently confirmed that the diffraction efficiency and the relief depth of the SRG is dramatically increased by corona charging at temperatures near or above T_g , and the SRG is not thermally erased above T_g [12]. This mechanism is not clear, but we think that the relief depth increases as a result of the Coulomb force exerted by the electric charge, and therefore the diffraction efficiency is increased. This increase effect depends on the corona charging conditions, specifically the corona charging temperature, the applied voltage and the corona charging time. This increase effect can be used to increase the initially low diffraction efficiency of the recorded hologram. We examined the increase in diffraction efficiency of the letters A and E as recorded by the Fourier transform hologram. Fourier hologram was recorded using the hologram recording setup shown in Fig. 2 and under the following conditions: The film thickness was about 1 μm . The recording power and time

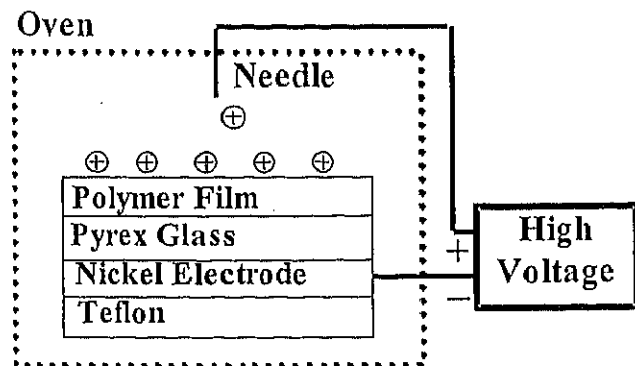
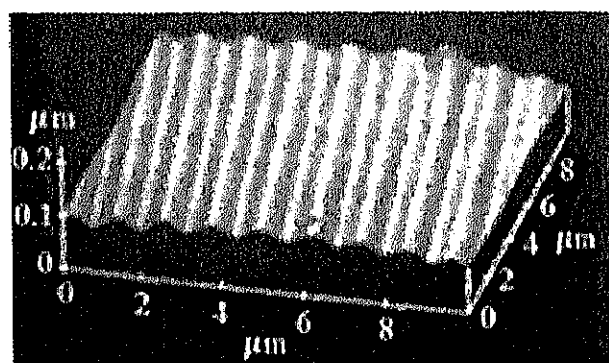


Fig. 4. Corona charging setup.

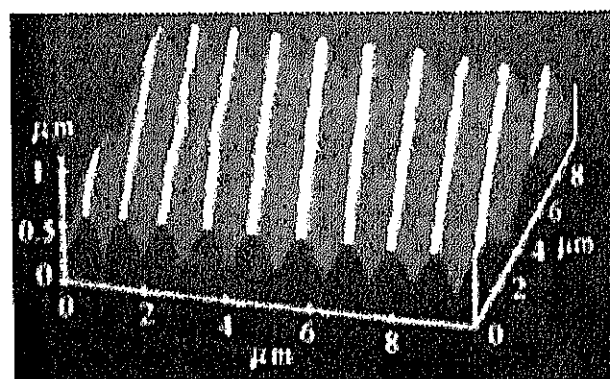
was $I_1 = I_2 = 88 \text{ mW/cm}^2$ and 1 min. The period of interference fringes was $1 \text{ }\mu\text{m}$. The electric charge was deposited on the hologram using a corona depositing poling setup in an oven shown in Fig. 4. The voltage was applied between the nickel electrodes and the needle electrodes, which was positioned 7 mm above the polymer film. In the corona charging process, the voltage was applied at a temperature near T_g and the polymer film was heated to the corona charging temperature with the voltage applied, because the SRG is thermally erased above T_g without the voltage applied. After the corona charging time, the polymer film was cooled to room temperature with the voltage applied. The corona charging conditions and the result are shown in Table 1. Fourier transform holograms were poled under two conditions. The only difference between the two conditions is the corona charging temperature. The first-order diffraction efficiency of a letter A measured before and after corona charging using a He-Ne laser beam with 1 mm diameter increased from 0.28% to 4.73% under Condition 1 and from

0.24% to 28.39% under Condition 2. For the letter E, the diffraction efficiency increased from 0.5% to 32.6%. The difference between the two results shows that this increase of the corona charging depends on the corona charging conditions and the diffraction efficiency of the hologram can control by corona charging conditions. The reconstructed images after corona charging are shown in Fig. 3(e) and (f). The reconstructed images of a letter A and E were clear and this means the damage caused by corona charging was not obvious.

Finally, we observed the recorded Fourier transform hologram using an atomic force microscope (AFM). The surface profiles of the Fourier transform hologram before and after corona charging are shown in Fig. 5(a) and (b). In this case, we used the letter A recorded under Condi-



(a)



(b)

Fig. 5. Surface profile of the Fourier transform hologram as measured by AFM (a) before corona charging; and (b) after corona charging.

Table 1
First-order diffraction efficiency before and after corona charging

	Condition 1	Condition 2	
Recording letter	A	A	E
Corona charging conditions	7 kV, 136°C, 20 min	7 kV, 141°C, 20 min	
Diffraction efficiency (%)			
Before	0.28	0.24	0.49
After	4.73	28.39	32.63

tion 2. The relief depths measured before and after corona charging were about 20 nm and about 350 nm, respectively. This shows that the increased diffraction efficiency caused by corona charging strongly depends on the increased relief depth of the recorded hologram. We have confirmed that the diffraction efficiency of the hologram increases dramatically as a result of corona charging and the maximum diffraction efficiency is over 30%. The first-order diffraction efficiency of the increased Fourier hologram remained unchanged for several months at room temperature under natural light. To our knowledge, this is the first example of the combination of the hologram recording by the photoinduced surface deformation and the increase effect by corona charging.

4. Conclusion

We have described Fourier transform hologram recording using the surface deformation technique. We have also proposed the corona charging method for increasing of the initially small diffraction efficiency of a recorded hologram. Using this increase effect, a hologram with high diffraction efficiency can be fabricated and the diffraction

efficiency of the hologram can be controlled by corona charging conditions.

References

- [1] J.F. Heanue, M.C. Bashaw, L. Hesselink, *Science* **265** (1994) 749.
- [2] S. Martin, C.A. Feely, V. Toal, *Appl. Opt.* **36** (1997) 5757.
- [3] K. Kawano, T. Ishii, J. Minabe, T. Niitsu, Y. Nishikata, K. Baba, *Opt. Lett.* **24** (1999) 1269.
- [4] D.Y. Kim, L. Li, X.L. Jiang, V. Shivshankar, J. Kumar, S.K. Tripathy, *Macromolecules* **28** (1995) 8835.
- [5] C.J. Barrett, A.L. Natansohn, P.L. Rochon, *J. Phys. Chem.* **100** (1996) 8836.
- [6] N.C.R. Holme, L. Nikolva, P.S. Ramanujam, S. Hvilsted, *Appl. Phys. Lett.* **70** (1997) 1518.
- [7] M. Itoh, K. Harada, H. Matsuda, S. Ohnishi, A. Parfenov, N. Tamaoki, T. Yatagai, *J. Phys. D: Appl. Phys.* **31** (1998) 463.
- [8] N.K. Viswanathan, S. Balasubramanian, L. Li, S.K. Tripathy, J. Kumar, *Jpn. J. Appl. Phys.* **38** (1999) 5298.
- [9] J. Kumar, L. Li, X.L. Jiang, D. Kim, T.S. Lee, S. Tripathy, *Appl. Phys. Lett.* **72** (1998) 2096.
- [10] C.J. Barrett, P.L. Rochon, A.L. Natansohn, *J. Chem. Phys.* **109** (1998) 1505.
- [11] D.Y. Kim, S.K. Tripathy, L. Li, J. Kumar, *Appl. Phys. Lett.* **66** (1995) 1166.
- [12] K. Munakata, K. Harada, H. Anji, M. Itoh, S. Umegaki, T. Yatagai, *Opt. Lett.* **26** (2001) 4.
- [13] K. Munakata, K. Harada, N. Yoshikawa, M. Itoh, S. Umegaki, T. Yatagai, *Opt. Rev.* **6** (1999) 518.

Diffraction efficiency increase by corona discharge in photoinduced surface-relief gratings on an azo polymer film

Katsuhiko Munakata, Kenji Harada, Hitoshi Anji, Masahide Itoh, and Toyohiko Yatagai

Institute of Applied Physics, University of Tsukuba and Tsukuba Advanced Research Alliance, Tennodai 1-1-1, Tsukuba, Ibaraki 305-8573, Japan

Shinsuke Umegaki

Faculty of Science and Technology, Keio University, Hiyoshi 3-14-1, Kohoku, Yokohama, Kanagawa 223-0061, Japan

Received August 3, 2000

The diffraction efficiency of a surface-relief grating (SRG) was dramatically increased by corona discharge. We fabricated this SRG by applying surface modulation to azo polymer films, using laser interference fringes. The electric charge was deposited upon the SRG by a corona discharge in an oven. The first-order diffraction efficiency measured before and after corona discharge above the glass-transition temperature increased from ~2% to ~40% in a SRG written with a circularly polarized beam. The relief depth of the SRG as measured with an atomic-force microscope also increased, from ~130 nm to ~450 nm. The increase in diffraction efficiency was independent of the writing polarization. © 2001 Optical Society of America

OCIS codes: 050.1950, 050.7330, 090.2900, 210.4770, 230.1950, 250.2080.

In the past several years, direct fabrication of relief structures in azo polymers has been reported.¹⁻³ This method is a one-step fabrication technique. A surface-relief grating (SRG) is fabricated by irradiation of interference fringes. This SRG has the following properties: It can be fabricated only upon azobenzene functionalized polymers such as side-chain- and main-chain-type azo polymers. The diffraction efficiency and the surface relief depth depend on the writing energy and the polarization of the writing laser beam.⁴ The fabrication temperature is below the glass-transition temperature (T_g), and this type of SRG is fabricated at room temperature upon a polymer with high T_g ($\approx 280^\circ\text{C}$). A large surface-relief depth ($>0.7\ \mu\text{m}$) has been reported. This form of SRG is highly stable at temperatures less than T_g and can be erased by heating above T_g . It can also be erased by laser irradiation below T_g , but this erasure is dependent on the polarization state.⁵ This fabrication mechanism is not well understood at present, but several models have been proposed.⁶⁻⁹

SRG fabrication with an azo polymer film has been reported.¹⁰ This type of SRG can be used as a passive grating element^{11,12} or a holographic element. However, the long fabrication time required for high diffraction efficiency is an obstacle to practical use of the SRG. It can however, be used as an active diffraction device when it is subjected to poling because the azo polymer film exhibits an electro-optic effect. The modulation of a surface-relief electro-optic grating with this SRG has also been reported.¹³

In this Letter we describe the diffraction-efficiency increase of a SRG caused by corona discharge. This increase is evaluated by the first-order diffraction efficiency and the relief depth of the SRG.

A SRG was fabricated by the irradiation of interference fringes on a side-chain-type azo polymer, Poly(orange Tom-1 isophoronedisocyanate).¹⁰ Polymer films of $\sim 1\text{-}\mu\text{m}$ thickness were prepared by spin coating

upon a Pyrex glass plate. The concentration of dye was 18 wt. %, and the T_g was 136°C . The refractive index was 1.61 at a wavelength of 633 nm. The light source was an Ar-ion laser beam with a wavelength of 488 nm. An electric charge was deposited upon the SRG in a corona-depositing poling setup in an oven. The voltage was applied between a nickel electrode and a needle electrode, which was positioned 7 mm above the polymer film. Electrons were released from the needle electrode by corona discharge. The temperature of the air in the oven was measured with a heat sensor. Changes in temperature and applied voltage during corona discharge are shown in Fig. 1. Voltage V_p was applied after the polymer film was heated to temperature T_p (usually T_p was set at T_g). When $T_p > T_g$, V_p was applied at a temperature near T_g . After time τ_p , the polymer film was cooled to room temperature T_0 with the voltage applied.

First we examined the change in the relief depth by heating the film without applied voltage so we could investigate the influence of the electric charge generated by the corona discharge. We observed this relief

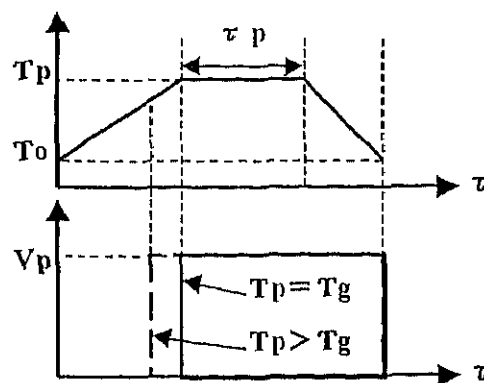


Fig. 1. Changes in temperature and applied voltage over time.

depth with an atomic-force microscope. The SRG was fabricated under the following conditions: writing by means of a circularly polarized beam, power of 50 mW/cm^2 , irradiation time of 15 min, and grating period of $1 \mu\text{m}$. The relief depth before heating was $130\text{--}160 \text{ nm}$. As a result of the heating of the SRG, the relief depth SRG was erased by $\sim 30\%$ under the conditions of $T_p = 136^\circ\text{C}$ and $\tau_p = 20 \text{ min}$ and was erased completely under the conditions of $T_p = 141^\circ\text{C}$ and $\tau_p = 20 \text{ min}$. We confirmed from the experiment that the SRG in the corona poling equipment was erased at temperatures above T_g .

Next we examined the change in diffraction efficiency as a result of corona discharge. The SRG was fabricated under the following conditions: writing by means of a circularly polarized beam, power of 50 mW/cm^2 , irradiation time of 10 min, and grating period of $1 \mu\text{m}$. The electric charge was deposited under the following conditions: $V_p = 8 \text{ kV}$ and $\tau_p = 20 \text{ min}$ were fixed, and T_p was changed. When $T_p \geq T_g$, V_p was applied at a temperature of 130°C . The temperature dependence of the first-order diffraction efficiency before and after corona discharge as measured by a He-Ne laser beam is shown in Fig. 2. In the polarization of the laser beam, s , 45° , and p polarization are equivalent to 0° (perpendicular to the grating vector), 45° , and 90° (parallel to the grating vector) polarization, respectively. No change in diffraction efficiency caused by corona discharge was detectable below 100°C , but a dramatic increase in diffraction efficiency was observed at temperatures near or above T_g . The first-order diffraction efficiency measured before and after corona discharge increased from $\sim 2\%$ to $\sim 40\%$. The experimental results demonstrated that the SRG was thermally erased above T_g without corona discharge but that the diffraction efficiency of the SRG was increased above T_g with corona discharge. This increase in diffraction efficiency can be caused by increased birefringence as a result of chromophore orientation caused by the electric field or by an increase in the relief depth caused by the electric charge or by both. We measured the surface profile of the SRG with an atomic-force microscope. The surface profiles before and after corona discharge under the condition $T_p = 141^\circ\text{C}$ are shown in Figs. 3(a) and 3(b), respectively. The relief depth before and after corona discharge increased from ~ 130 to $\sim 450 \text{ nm}$. This means that the increased diffraction efficiency that results from corona discharge depends strongly on the increased relief depth of the SRG.

We examined the relation between the increase in diffraction efficiency caused by corona discharge and the diffraction efficiency before corona discharge. The irradiation-time dependence of the first-order diffraction efficiency before and after corona discharge is shown in Fig. 4. The fabrication conditions for the SRG were the same as described above, except that $T_p = 141^\circ\text{C}$ was fixed and the irradiation times were changed. The diffraction efficiency of the SRG fabricated by an irradiation time of 2 min was increased sufficiently by corona discharge. In this case, the first-order diffraction efficiency for the 45° -polarized

beam increased from $\sim 0.22\%$ to $\sim 36\%$. The diffraction efficiency in the case of a shorter irradiation

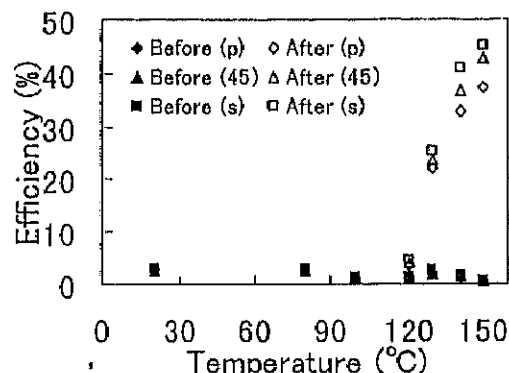
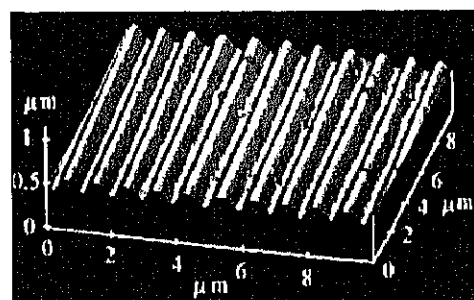
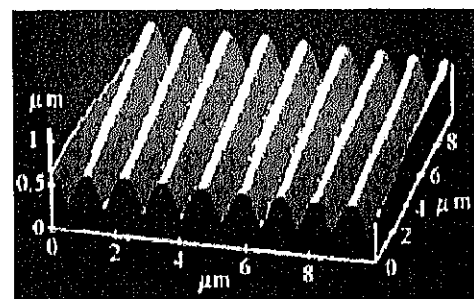


Fig. 2. Poling-temperature dependence of the first-order diffraction efficiency for p -, 45° -, and s -polarized beams before and after corona discharge.



(a)



(b)

Fig. 3. Surface profile of the SRG measured with an atomic-force microscope (a) before and (b) after corona discharge.

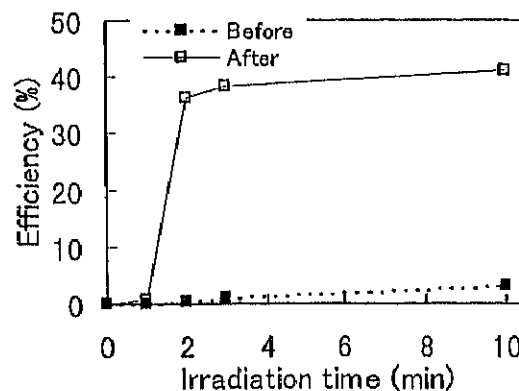


Fig. 4. Irradiation-time dependence of the first-order diffraction efficiency for a 45° -polarized beam before and after corona discharge.

Table 1. Diffraction Efficiency Before and After Corona Discharge of a SRG Written by Differently Polarized Beams

Polarization State of Writing Beam	Diffraction Efficiency (%)	
	Before Discharge	After Discharge
Circular	8.2	18.6
<i>p</i>	4.7	10.8
45°	7.7	17.1
<i>s</i>	0.02	0.23

time (1 min), however, was increased only from 0.07% to 0.83%. This result shows that a critical relief depth is necessary for an increase in the diffraction efficiency of a SRG. The relief depth of the SRG that demonstrates a diffraction efficiency of 0.22% is ~30 nm.

The process of SRG fabrication depends strongly on polarization⁴ and the polymer film becomes birefringent with the chromophores preferentially oriented. Finally, therefore, we examined the diffraction-efficiency increase in SRG's fabricated by different polarization beams. SRG's, were fabricated under the following conditions: power of 50 mW/cm²; irradiation time of 10 min; grating period of 1 μ m. With respect to the polarization state of the laser beam, the circular polarization state, *p* polarization, 45° polarization, and *s* polarization were used. The electric charge was deposited under the following conditions: $V_p = 8$ kV, $\tau_p = 20$ min, and $T_p = 136$ °C. The experimental results are detailed in Table 1. The polarization of the readout He-Ne laser beam was 45°. The diffraction efficiency of the SRG fabricated with all polarization states used was increased by corona discharge, which shows that the mechanism by which diffraction efficiency increases is independent of the polarization state of the writing laser beam.

Our experimental results indicate that the change in a SRG cause by corona discharge has the following characteristics: (1) A dramatic increase in diffraction efficiency and relief depth are observed at temperatures near or above T_g , and the SRG is not thermally erased above T_g . (2) Increasing the relief depth and the diffraction efficiency of the SRG in a short time requires a critical relief depth. (3) This increase does not depend on the polarization state of the writing laser beam. We speculate that the mechanism that leads to an increase in diffraction efficiency caused by corona discharge is similar to that for thermoplastic film.¹⁴ We conclude that, when a SRG with a fine period is exposed to a corona discharge, an electric charge collects in the groove area because the relief depth is increased even if the polymer film becomes

soft above T_g . The relief depth increases as a result of the Coulomb force exerted by the electric charge, and therefore the diffraction efficiency is increased. However, chromophore orientation caused by the electric field may also influence this effect. The effects described here have not yet been experimentally proved. Further experiments will be necessary to elucidate the mechanism fully.

In conclusion, we have described the increase in the diffraction efficiency and the relief depth of a surface-relief grating caused by corona discharge. The first-order diffraction efficiency measured before and after the corona discharge increased from ~2% to ~40% in a SRG written with a circularly polarized beam. This increase was independent of the writing polarization of the SRG but depended on the relief depth. Using this increase effect, one could fabricate a SRG or a surface-relief electro-optic grating with high diffraction efficiency at a relatively low writing power.

This research was partly supported by a grant-in-aid for scientific research from the Ministry of Education, Science, Sports and Culture of Japan and by the Yata-gai Project, Tsukuba Advanced Research Alliance, University of Tsukuba. K. Munakata's e-mail address is munakata@optlab2.bk.tsukuba.ac.jp.

References

1. D. Y. Kim, L. Li, X. L. Jiang, V. Shivshankar, J. Kumar, and S. K. Tripathy, *Macromolecules* **28**, 8835 (1995).
2. C. J. Barrett, A. L. Natansohn, and P. L. Rochon, *J. Phys. Chem.* **100**, 8836 (1996).
3. N. C. R. Holme, L. Nikolva, P. S. Ramanujam, and S. Hvilsted, *Appl. Phys. Lett.* **70**, 1518 (1997).
4. X. L. Jiang, L. Li, J. Kumar, D. Y. Kim, V. Shivshankar, and S. K. Tripathy, *Appl. Phys. Lett.* **68**, 2618 (1996).
5. X. L. Jiang, L. Li, J. Kumar, D. Y. Kim, and S. K. Tripathy, *Appl. Phys. Lett.* **72**, 2502 (1998).
6. T. G. Pedersen, P. M. Johansen, N. C. R. Holm, P. S. Ramanujam, and S. Hvilsted, *Phys. Rev. Lett.* **80**, 89 (1997).
7. J. Kumar, L. Li, X. L. Jiang, D. Y. Kim, T. S. Lee, and S. Tripathy, *Appl. Phys. Lett.* **72**, 2096 (1998).
8. C. J. Barrett, P. L. Rochon, and A. L. Natansohn, *J. Chem. Phys.* **109**, 1505 (1998).
9. K. Sumaru, T. Yamanaka, T. Fukuda, and H. Matsuda, *Appl. Phys. Lett.* **75**, 1878 (1999).
10. M. Itoh, K. Harada, H. Matsuda, S. Ohnishi, A. Parfenov, N. Tamaoki, and T. Yatagai, *J. Phys. D* **31**, 463 (1998).
11. J. Paterson, A. Natansohn, P. Rochon, C. L. Callender, and L. Robitaille, *Appl. Phys. Lett.* **69**, 3318 (1996).
12. P. Rochon, A. Natansohn, C. L. Callender, and L. Robitaille, *Appl. Phys. Lett.* **71**, 1008 (1997).
13. K. Munakata, K. Harada, N. Yosikawa, M. Itoh, S. Umegaki, and T. Yatagai, *Opt. Rev.* **6**, 518 (1999).
14. J. C. Urbach and R. W. Meier, *Appl. Opt.* **5**, 666 (1966).

Holographic Recording and Control of Diffraction Efficiency Using Photoinduced Surface Deformation on Azo-Polymer Films

Kenji HARADA*, Hajime INOUE, Mohamed A. EL-MORSY¹, Masahide ITOH,
 Shinsuke UMEGAKI² and Toyohiko YATAGAI

Institute of Applied Physics and Tsukuba Advanced Research Alliance (TARA), University of Tsukuba, Tsukuba 305-8573, Japan

¹*Physics Department, Faculty of Science, Damietta, University of Mansoura, Damietta, Egypt*

²*Faculty of Science and Technology, Keio University, Hiyoshi, Yokohama 223-0061, Japan*

(Received October 1, 2001; accepted for publication October 30, 2001)

Surface relief holograms were fabricated on azo-polymer films by the irradiation of interference laser fringes. The side-chain azo-polymer, poly-orange tom-1 isophoronedisocyanate, was used in this study. Recording characteristics of surface relief structures were investigated; they needed no post-treatment, and could be erased by heating or irradiating a uniform laser beam. The diffraction efficiency of the recorded hologram was markedly increased by corona charging. It was also controlled by irradiation of the laser beam (488 nm) with corona charging. [DOI: 10.1143/JJAP.41.1851]

KEYWORDS: hologram, azo-polymer, photoinduced surface deformation, surface relief grating, corona charging

1. Introduction

Polymeric materials are the most promising organic materials for electrooptic devices and memory devices. The recording of polarization holographic gratings using azobenzene-containing polymer films as photoanisotropic materials has been reported.¹⁾ This photoinduced anisotropic effect is due to trans-cis-trans isomerization and the orientational effects of the azo-dye chromophore. Direct fabrication of relief structures in azo-polymers has been reported in the past several years.^{2–5)} A surface relief structure is recorded through photoisomerization and the movements of the polymer chains.^{6,7)} This is a one-step fabrication technique. A surface relief structure is fabricated by irradiation of interference laser fringes onto azobenzene functionalized polymers such as side-chain-type and main-chain-type azo-polymers. The diffraction efficiency and the surface relief depth depend on the writing energy and the polarization of the writing laser beam.⁸⁾ This structure is very stable at temperatures below the glass transition temperature T_g and can be erased by heating above T_g . This fabrication mechanism is not well understood at present, but several models have been proposed.^{9–12)}

We have recently reported that the diffraction efficiency of the surface relief structure can be markedly increased by corona charging.¹³⁾ Moreover, such a hologram exhibits non-linearity, because the orientation of the azo chromophore and the increase in the diffraction efficiency are performed concurrently by corona charging. Surface relief grating fabrication and the modulation of a surface relief electrooptic grating have been reported.¹⁴⁾

In this paper, surface relief holograms are fabricated on azo-polymer films by irradiation of interference laser fringes. The diffraction efficiency of the hologram is controlled by irradiation of the laser beam with corona charging.

2. Surface Deformation Method

The side-chain azo-polymer, poly-orange tom-1 isophoronedisocyanate, is used in this study. Figure 1 shows the chemical structure and absorption spectrum of the material.

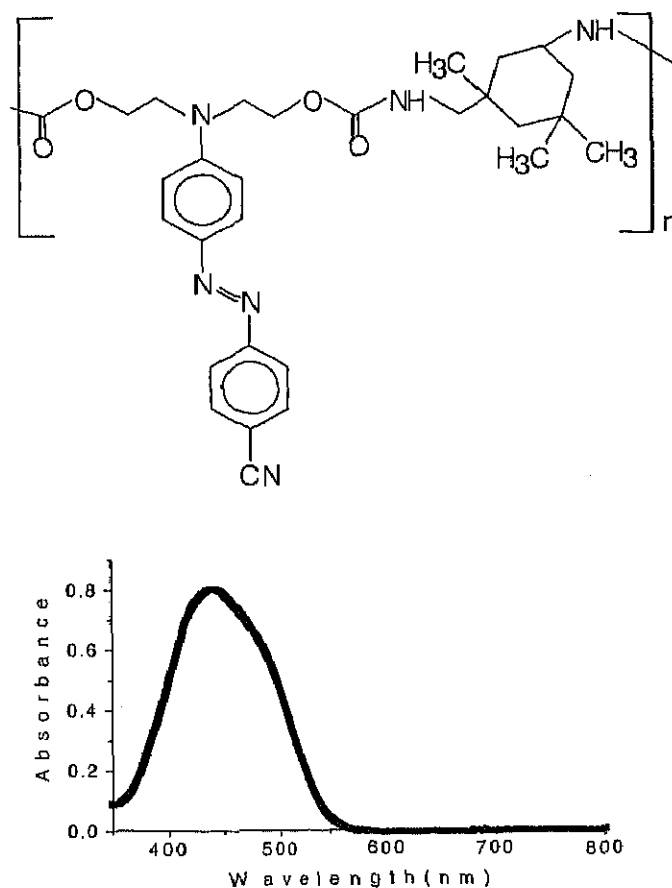


Fig. 1. Chemical structure and absorption spectrum of the material.

rial. The glass transition temperature is 136°C. The absorption peak and the cut-off wavelength of the dye are 440 nm and 560 nm, respectively. This polymer is dissolved in cyclohexanone. Samples of 1–5 μm thickness are prepared by spin-coating on a slide glass plate. The refractive index of the film is measured as 1.65 at a wavelength of 633 nm by the m-line technique.

The surface relief grating is fabricated by the irradiation of two-beam interference fringes. The experimental setup is

*E-mail address: harada@optlab2.bk.tsukuba.ac.jp

shown in Fig. 2. A polarized Ar-ion laser beam at a wavelength of 488 nm is used as the light source. The laser beam is collimated to 6 mm in diameter, half of the laser beam is reflected by a mirror and the two beams interfere on the sample. The setup is strong arrangement in the vibration. The angle between the sample and the mirror is 90° and the period of the grating can be adjusted by varying the angle between θ the beam propagation axis and the mirror plane. Figure 3 shows the polarization dependence of the diffraction efficiency. The period of the surface relief grating is selected as $1 \mu\text{m}$. There is a strong polarization dependence of the writing laser beam. High diffraction efficiency is obtained using a p- or circularly polarized writing beam. The relief structure is not recorded using an s-polarized writing beam. A high diffraction efficiency can be obtained in a short time by high-power recording.¹³⁾ Figure 4 shows an atomic force microscopy image of

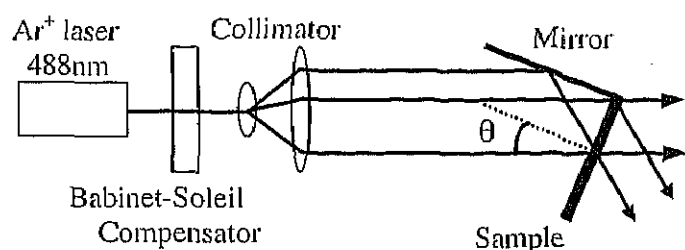


Fig. 2. Optical setup for surface relief grating fabrication by the surface deformation method.

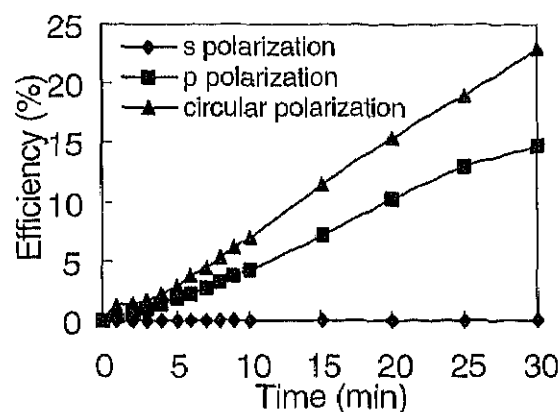


Fig. 3. Polarization dependence of the diffraction efficiency.

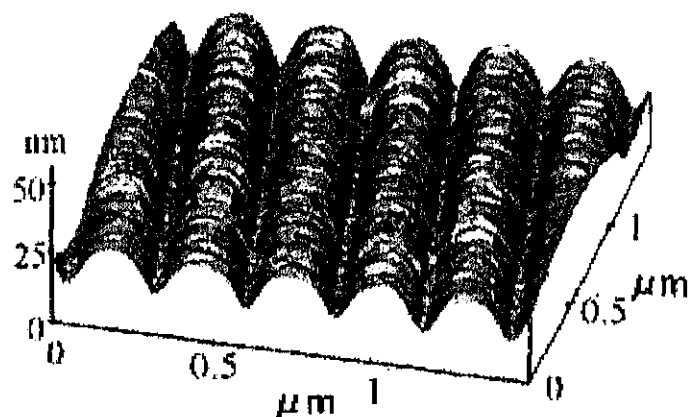


Fig. 4. Atomic force microscopy image of surface relief structure.

a surface relief structure recorded using a p-polarized beam. The laser beam power was 220 mW/cm^2 for 10 min. A minimum relief period of 275 nm was recorded. The surface relief depth was 16 nm.

3. Recording of Fourier Transform Hologram

Next, we examined Fourier transform hologram recording using the photoinduced surface modulation technique. The hologram recording setup is shown in Fig. 5. A circularly polarized Ar-ion laser beam with a wavelength of 488 nm was used. The laser beam was collimated to a 6 mm diameter and separated by a beam splitter. The Fourier transform hologram was recorded on an azo-polymer film with a thickness of about $2 \mu\text{m}$. The letter A, 4 mm tall and 3 mm wide, was used as the object. The beam power in front of the object was $I_1 = 118 \text{ mW/cm}^2$. The object beam was Fourier transformed on the azo-polymer film using a lens with a focal length of 100 mm. The reference beam power was $I_2 = 118 \text{ mW/cm}^2$ and the recording time was 1 min. The reconstructed image is shown in Fig. 6(a). This reconstructed image was observed using a He-Ne laser beam. The diffraction efficiency of the recorded hologram measured using a He-Ne laser was 1.2%.

4. Diffraction Efficiency Control of the Hologram

We have recently confirmed that the diffraction efficiency and the relief depth of a surface relief structure is markedly increased by corona charging at temperatures near or above its T_g .¹³⁾ The mechanism is not clearly understood, but we consider that the relief depth increases as a result of the Coulomb force exerted by electric charge; therefore the diffraction efficiency is increased. This increase depends on the corona

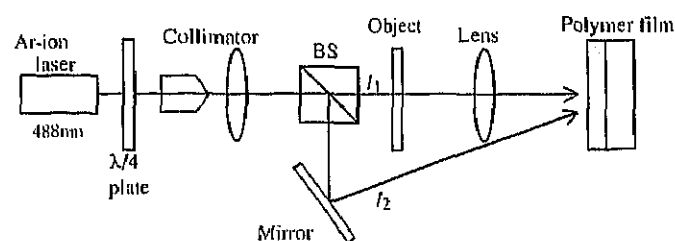


Fig. 5. Experimental setup for Fourier transform hologram recording.

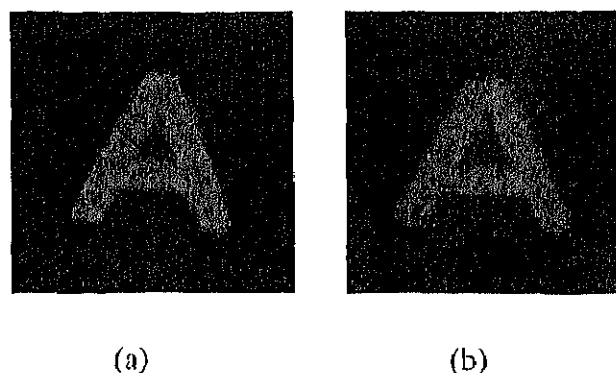


Fig. 6. The reconstructed images (a) before corona charging and (b) after corona charging.

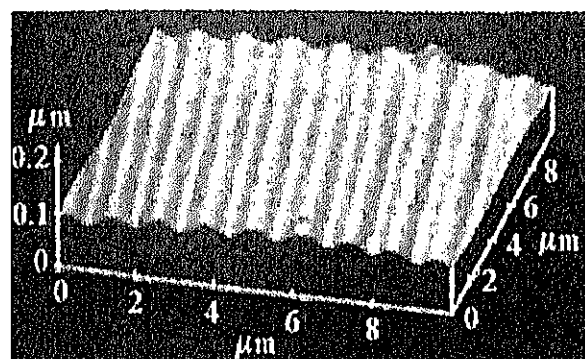
charging conditions, specifically, the corona charging temperature, the applied voltage and the corona charging time. The increase can be used to increase the initially low diffraction efficiency of the recorded hologram. We examined the increase in diffraction efficiency of the letter A recorded by the Fourier transform hologram. The Fourier transform hologram was recorded using the hologram recording setup shown in Fig. 5. The recording power and time were $I_1 = I_2 = 88 \text{ mW/cm}^2$ and 1 min, respectively. The period of interference fringes was $1 \text{ }\mu\text{m}$.

The electric charge was deposited on the hologram using a corona deposition poling setup in an oven. A sharp needle electrode was positioned above the ground electrodes. The hologram was placed on the ground electrode. The distance between the polymer film and the needle electrode was 7 mm.

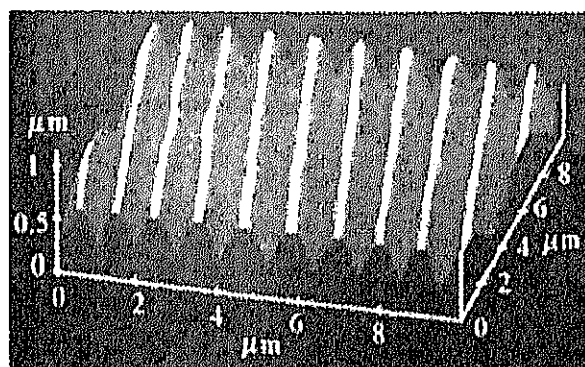
In the corona charging process, the voltage was applied at a temperature near T_g and the polymer film was heated to the corona charging temperature with the voltage applied, because the surface relief structure is thermally erased above T_g without the applied voltage. After corona charging for 20 min, the polymer film was cooled to room temperature with the applied voltage. During the corona charging process, a voltage of 7 kV was applied at 141°C . The first-order diffraction efficiency of the hologram measured before and after corona charging using a He-Ne laser increased from 0.24% to 28.39%. This increase in the corona charging depends on the corona charging conditions, and the increase in the diffraction efficiency of the hologram can be controlled by these conditions. The reconstructed images after corona charging are shown in Fig. 6(b).

We observed the recorded Fourier transform hologram using an atomic force microscope (AFM). The surface profiles of the Fourier transform hologram before and after corona charging are shown in Figs. 7(a) and 7(b). The relief depths measured before and after corona charging were about 20 nm and about 350 nm, respectively. This indicates that the increased diffraction efficiency caused by corona charging strongly depends on the increased relief depth of the recorded hologram. We have confirmed that the diffraction efficiency of the hologram increases markedly as a result of corona charging, and the maximum diffraction efficiency is over 30%. The first-order diffraction efficiency of the increased Fourier hologram remained unchanged for several months at room temperature under natural light.

Next, the diffraction efficiency was controlled by the irradiation of the laser beam. A circularly polarized laser beam was irradiated onto the hologram with corona charging at 141°C . The reflected first-order diffraction efficiency of the He-Ne laser was detected. Figure 8 shows the *in situ* measurement of the diffraction efficiency control of the hologram. At $t = 0 \text{ s}$, the electric charge was deposited on the hologram at 130°C . The applied voltage was 6.5 kV. At $t = 20 \text{ s}$, the hologram was heated to 150°C with corona charging. Diffraction efficiency increased upon heating the sample to above its T_g with corona charging. At $t = 90 \text{ s}$, a uniform Ar-ion laser beam of about 5 mW/cm^2 was irradiated onto the hologram. The increase in the diffraction efficiency became slower. At $t = 130 \text{ s}$, uniform Ar-ion laser beam of about 50 mW/cm^2 was irradiated onto the hologram and the diffraction efficiency decreased. At $t = 150 \text{ s}$, the Ar-ion laser beam was



(a)



(b)

Fig. 7. Surface profiles of the Fourier transform hologram (a) before corona charging and (b) after corona charging.

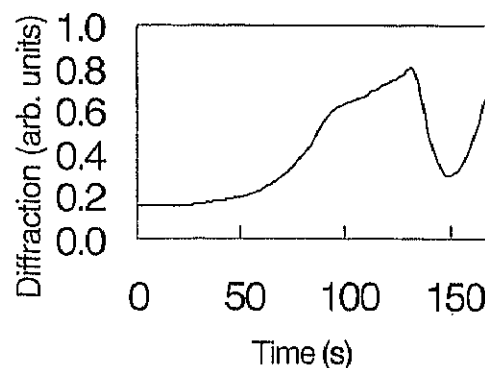


Fig. 8. Diffraction efficiency control of the hologram.

turned off and the diffraction efficiency increased again.

Thus, the diffraction efficiency was increased by the corona charging, and decreased by the laser beam irradiation with corona charging. We can control the diffraction efficiency of the surface relief hologram by controlling the irradiation power of the laser beam. To our knowledge, this is the first example of diffraction efficiency control of a surface relief hologram by the irradiation of a laser beam with corona discharge.

5. Conclusions

We proposed a new hologram recording technique using photoinduced surface deformation on azo-polymer films. The first-order diffraction efficiency of the hologram increased from 0.24% to 28.39%. The diffraction efficiency was controlled by the irradiation of a uniform laser beam at a wavelength of 488 nm with corona charging. This recording technique can be applied to holographic memory devices.

Acknowledgments

This research was partly supported by a Grant-in-Aid for Scientific Research from the Ministry of Education, Culture, Sports, Science and Technology and by the Yatagai Project, Tsukuba Advanced Research Alliance, University of Tsukuba.

- 1) K. Kawano, T. Ishii, J. Minabe, T. Niitsu, Y. Nishikata and K. Baba: *Opt. Lett.* **24** (1999) 1269.
- 2) D. Y. Kim, L. Li, X. L. Jiang, V. Shivshankar, J. Kumar and S. K.

- Tripathy: *Macromolecules* **28** (1995) 8835.
- 3) C. J. Barrett, A. L. Natansohn and P. L. Rochon: *J. Phys. Chem.* **100** (1996) 8836.
- 4) N. C. R. Holme, L. Nikolova, P. S. Ramanujam and S. Hvilsted: *Appl. Phys. Lett.* **70** (1997) 1518.
- 5) M. Itoh, K. Harada, H. Matsuda, S. Ohashi, A. Parfenov, N. Tamaoki and T. Yatagai: *J. Phys. D: Appl. Phys.* **31** (1998) 463.
- 6) C. J. Barrett, P. L. Rochon and A. L. Natansohn: *J. Chem. Phys.* **109** (1998) 1505.
- 7) D. Y. Kim, S. K. Tripathy, L. Li and J. Kumar: *Appl. Phys. Lett.* **66** (1995) 1166.
- 8) X. L. Jiang, L. Li, J. Kumar, D. Y. Kim, V. Shivshankar and S. K. Tripathy: *Appl. Phys. Lett.* **68** (1996) 2618.
- 9) T. O. Pedersen, P. M. Johansen, N. C. R. Holm, P. S. Ramanujam and S. Hvilsted: *Phys. Rev. Lett.* **80** (1997) 89.
- 10) J. Kumar, L. Li, X. L. Jiang, D. Y. Kim, T. S. Lee and S. Tripathy: *Appl. Phys. Lett.* **72** (1998) 2096.
- 11) C. J. Barrett, P. L. Rochon and A. L. Natansohn: *J. Chem. Phys.* **109** (1998) 1505.
- 12) K. Sumaru, T. Yamanaka, T. Fukuda and H. Matsuda: *Appl. Phys. Lett.* **75** (1999) 1878.
- 13) K. Munakata, K. Harada, H. Anji, M. Itoh, S. Umegaki and T. Yatagai: *Opt. Lett.* **26** (2001) 4.
- 14) K. Munakata, K. Harada, N. Yoshikawa, M. Itoh, S. Umegaki and T. Yatagai: *Opt. Rev.* **6** (1999) 518.

Multiple-Beam Fizeau Fringe-Pattern Analysis Using Fourier Transform Method for Accurate Measurement of Fiber Refractive Index Profile of Polymer Fiber

M. A. EL-MORSY,¹ T. YATAGAI,¹ A. HAMZA,² M. A. MABROUK,³ T. Z. N. SOKKAR²

¹ Institute of Applied Physics, Yatagai Laboratory, University of Tsukuba, Tsukuba, Ibaraki 305-5873, Japan

² Physics Department, University of Mansoura, Mansoura, Egypt

³ Physics Department, Damietta, University of Mansoura, Damietta, Egypt

Received 30 March 2001; accepted 16 June 2001

Published online 10 May 2002 in Wiley InterScience (www.interscience.wiley.com). DOI: 10.1002/app.10387

ABSTRACT: In this article the Fourier transform method is applied to analyze multiple-beam interference Fizeau fringes. The real part of the inverse Fourier transform is used to estimate a theoretical pattern. This pattern coincides with the experimental one. A derivative-sign binary image of the interference pattern is also used in automated determination of the contour line of the fringe pattern, regardless of the quality of this pattern. A correlation between the pixel size and the accuracy of the measured fiber refractive index is presented. © 2002 Wiley Periodicals, Inc. *J Appl Polym Sci* 85: 475–484, 2002

Key words: multiple-beam Fizeau fringes; refractive index profile; polyethylene fiber; fringe analysis; Fourier transform

INTRODUCTION

The study of the optical properties of fibers is a valuable task in fiber research because their structural characteristics are manifested in their optical properties. There are many parameters that affect the characteristics of optical fibers, such as the fiber radius, refractive index profile, numerical aperture, material dispersion, and attenuation. The refractive index profile and material dispersion have strong effects on the group delay characteristics of an optical fiber.¹ The values of the refractive indices of textile fibers, using plane polarized monochromatic light vibrating parallel and perpendicular to the fiber axis, give

useful information about the molecular arrangement of these fibers. They can also provide information about the structural and mechanical properties of these fibers. Thus, refractive index measurements using accurate methods have been studied by numerous authors.^{2–9}

Different techniques have been developed to determine the fiber refractive index profile. All of these techniques have their own advantages and disadvantages. The ideal measuring technique should be nondestructive and applicable to any preform and have high accuracy, high resolution, and easy measurement and processing of data.¹⁰

The multiple-beam Fizeau fringe system is a sensitive optical technique, and it needs no special sample preparation for measuring the refractive index profile of textile and optical fibers.^{2,7,8,11} Interference fringes are formed across the fiber when immersed in a silvered liquid

Correspondence to: M. A. El-Morsey (elmorsey@optlab2.bk.tsukuba.ac.jp or elmorsym@yahoo.com).

Journal of Applied Polymer Science, Vol. 85, 475–484 (2002)
© 2002 Wiley Periodicals, Inc.

wedge interferometer illuminated by a parallel beam of monochromatic light. The shift in the position of the interference fringe is formed because the fiber inside the interferometer works as a phase object. The value of this shift depends on the optical properties of the fiber. It gives quantitative information about the optical properties of the fiber under test and its structure. The methods in which matching immersion liquids are used give good results for the fiber refractive index profiles, especially when liquid and fiber cladding both have refractive indices close to each other. However, to minimize the error in the measured data, it is essential to take into consideration the effect of refraction of the beam through the liquid-fiber and core-cladding interfaces.^{4,7,12} The manual work for processing multiple-beam Fizeau fringes is however time consuming, cumbersome, and error prone because the interferogram must be photographed, enlarged to a suitable magnification, and the measured quantities then obtained from the magnified image.

Automated, high-speed image-processing techniques are used to analyze the fringe pattern and give an accurate analysis. The main procedure in automatic fringe-pattern analysis is fringe skeleton extraction. Several investigators¹³⁻¹⁹ proposed various digital image-processing algorithms for extracting fringe skeletons from the fringe patterns. This process can be classified into two categories. In the first category the fringe field is identified as a binary image and the fringe skeletons are obtained using algorithms that were primarily developed for optical character recognition. A recently published article⁸ comes under this category. In the second category the intensity variation within a fringe is used in devising algorithms for fringe skeleton determination. The algorithm applied by Yatagai et al.¹³ comes under this category.

One of the biggest problems involved in practical digital fringe-pattern analysis is the noise reduction problem, regardless of what type of image-processing method is used. Without noise the fringe-pattern analysis is much easier to analyze and is usually straightforward. Unfortunately, during the acquisition and digitization of the fringe pattern various noises appear in the digital fringe patterns. We applied a Fourier transform (FT) passband filter to reduce the pattern's noise.

The main focus in this work is to analyze the multiple-beam Fizeau fringe pattern using 1-dimensional (1-D) FT for accurate measurement of

the refractive index profile of a polyethylene polymer fiber.

THEORETICAL

Refractive Index Profile

Interference methods are used to determine the refractive index distribution along the fiber radius from the lateral shift of the interference fringe, which gives the phase shift of light passing through it. The fiber cross section is assumed to be divided into N circular zones. For a large number of layers, each layer can be considered to have a constant refractive index. The interference fringe shift (Z_Q) of the Q th layer in the fiber region is related to the refractive index (n_Q) of the layer as

$$\begin{aligned} \frac{\lambda Z_Q}{2h} = & \sum_{j=1}^{Q-1} 2n_j \left\{ \sqrt{(R - (j-1)a)^2 - \left(\frac{d_Q n_o}{n_j}\right)^2} \right. \\ & \left. - \sqrt{(R - ja)^2 - \left(\frac{d_Q n_o}{n_j}\right)^2} \right\} \\ & + 2n_Q \sqrt{(R - (Q-1)a)^2 - \left(\frac{d_Q n_o}{n_j}\right)^2} \\ & - n_o \{ \sqrt{R^2 - d_Q^2} + \sqrt{R^2 - X_Q^2} \} \quad (1) \end{aligned}$$

where λ is the wavelength of the light used, h is the interfering space, R is the fiber radius, a is the layer thickness ($a = R/N$), $n_o = n_L$ is the immersion liquid refractive index, and X_Q and d_Q are the emergent and incident ray distances from the fiber center, respectively, where

$$\begin{aligned} d_Q &= \frac{n_Q \left(R - \left(Q - \frac{1}{2} \right) a \right)}{n_o} \\ X_Q &= R \sin(\beta_Q) \\ \beta_Q &= 2 \sum_{j=0}^{Q-1} (\alpha_j - \theta_j) + \theta_o \quad (2) \end{aligned}$$

where β is the angle between the radius at the ray exit point and the incident ray and θ and α are the incidence and refraction angle, respectively.⁷ Using eq. (1) and the Z_Q value a computer program was prepared to measure the refractive index pro-

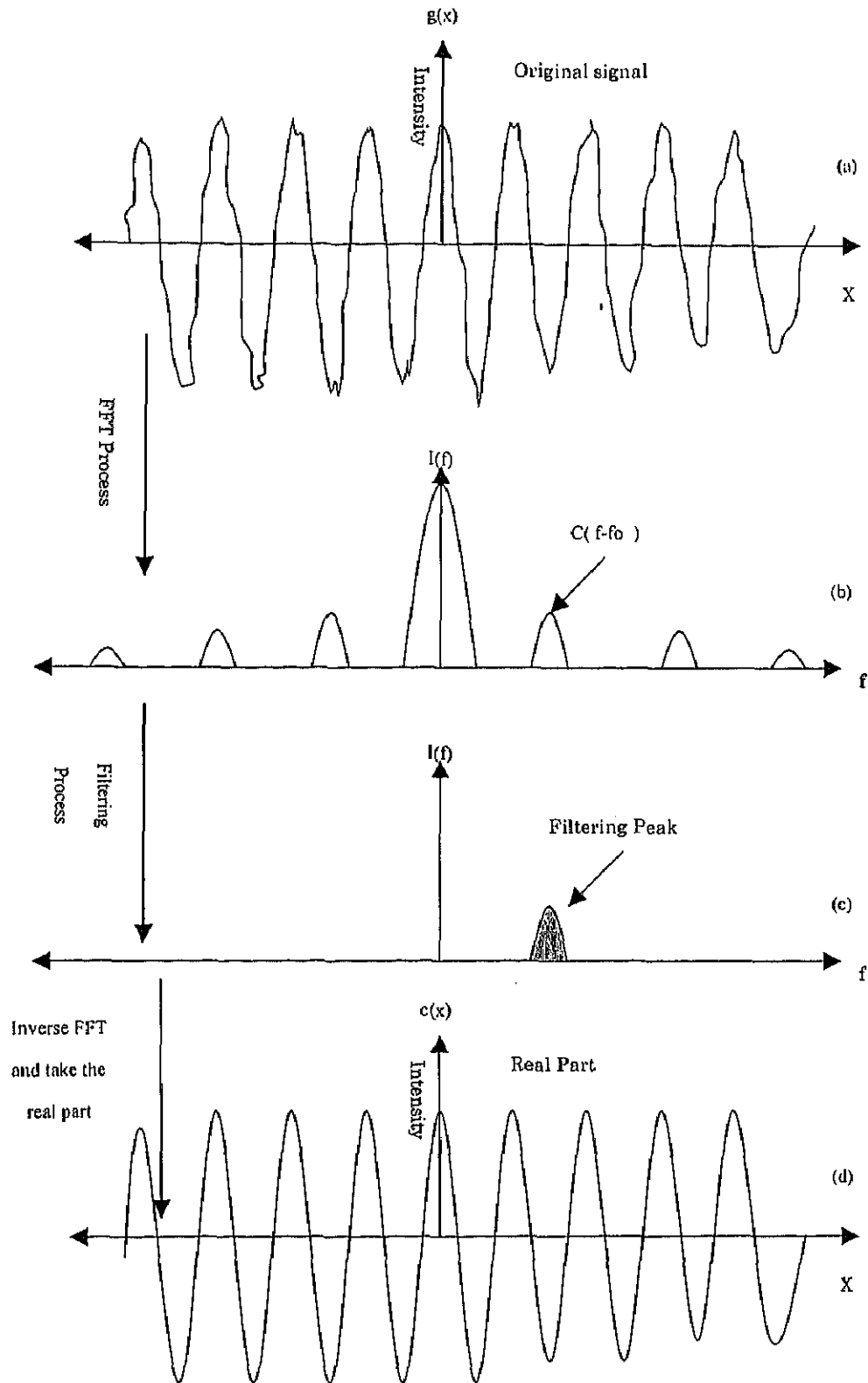


Figure 1 A schematic diagram of 1-dimensional (1-D) filtering: (a) the original 1-D relatively noise-free fringe pattern, (b) the modulus of the Fourier transform of the original, (c) filtering of the desired peak of the former, and (d) the real part of the inverse Fourier transform.

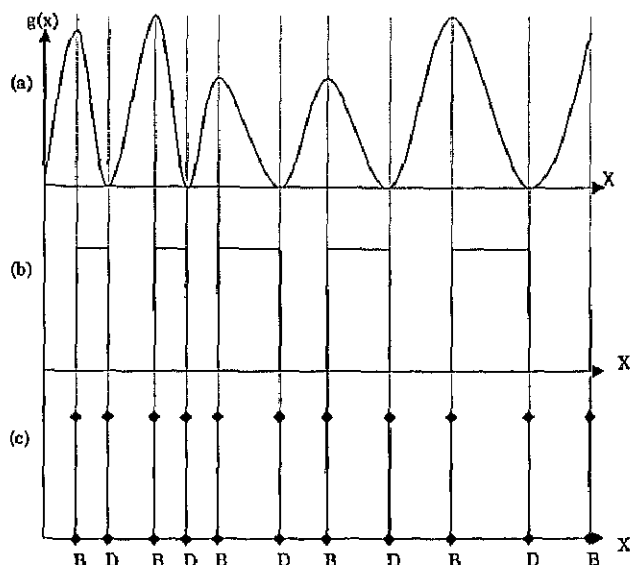


Figure 2 A schematic diagram of a derivative-sign binary fringe pattern: (a) the intensity distribution of the interference fringe pattern, (b) the intensity distribution of the derivative-sign binary fringe pattern of the former, and (c) the fringe skeleton; B, bright; D, dark.

file of the fibers. The accuracy of this profile depends on the accuracy of the fringe shift measurement. The following section deals with the methods of fringe shift data refinement.

Fourier Filtering

Interference periodic fringe and their Fourier spectra occur quite frequently in optics. The FT method of fringe-pattern analysis is useful in removing the noise from the fringe pattern. Fourier fringe analysis was originally introduced and demonstrated by Takeda et al.^{20,21} The technique was also studied by many others.²²⁻²⁵ The intensity data contained in such a fringe pattern can be written as

$$g(x) = a(x) + b(x)\cos(2\pi f_0 x + \phi(x)) \quad (3)$$

where $a(x)$ represents the background variations, $b(x)$ describes variations in the fringe visibility, $\phi(x)$ is the phase of the object, and f_0 is the carrier frequency. This equation can be rewritten as

$$g(x) = a(x) + c(x)\exp(i2\pi f_0 x) + c^*(x)\exp(-i2\pi f_0 x) \quad (4)$$

where

$$c(x) = \frac{1}{2} b(x)\exp(i\phi(x))$$

and $c^*(x)$ denotes complex conjugation of $c(x)$.

Using the FT algorithm, we compute the 1-D FT of eq. (4) for the variable x as shown in Figure 1 and y is fixed.

$$G(f) = A(f) + C(f - f_0) + C^*(-f - f_0) \quad (5)$$

where the capital letters denote Fourier spectra, f is the variable in spatial frequency space, and $C(f - f_0)$ is the FT of $c(x)$ with respect to x . From eq. (5) one can notice that $a(x)$, $b(x)$, and $\phi(x)$ are slowly varying functions compared to the variations introduced by the f_0 . Thus, when the FT of the fringe pattern is taken, three peaks are obtained as shown in Figure 1. The FT of the term $A(f)$ is placed in the center of the spectrum and the FTs of $C(f - f_0)$ and $C^*(f - f_0)$ will be symmetric with respect to the center and placed at a distance that is determined by f_0 .^{26,27} We make use of either of the two peaks' spectra on the carrier, say $C(f - f_0)$. In other words, the unwanted peaks are filtered out in this step. Using the inverse FT (IFT), if we compute the IFT of $C(f - f_0)$ with respect to f , then the term $c(x)$ itself will be obtained. The real part of $c(x)$ represents the filtered image pattern.

Image Skeleton (Fringe Centers)

The location of the geometric fringe centers can be determined by two methods. The first method uses a thinning algorithm; the disadvantage of this algorithm is that it usually requires numerous iterations in order to peel the fringe pattern. The second method consists of differential filter techniques.^{18,19} This algorithm is very simple because it requires one step to find the center of the fringe pattern and is suitable for straight, circular, or any type of fringe pattern. More explanations about the differential filter techniques are given in the following text.

Regardless of how dark or bright the interference fringes are and no matter what the fringe density, one of the most characteristic of the interferometric fringe patterns is that the derivatives in the fringe normal direction on both sides of a fringe centerline have opposite signs. We used this feature to determine the derivative-sign binary image of a fringe pattern. In the binary image, if the derivative signs of the original fringe pattern of the points are positive, the points are

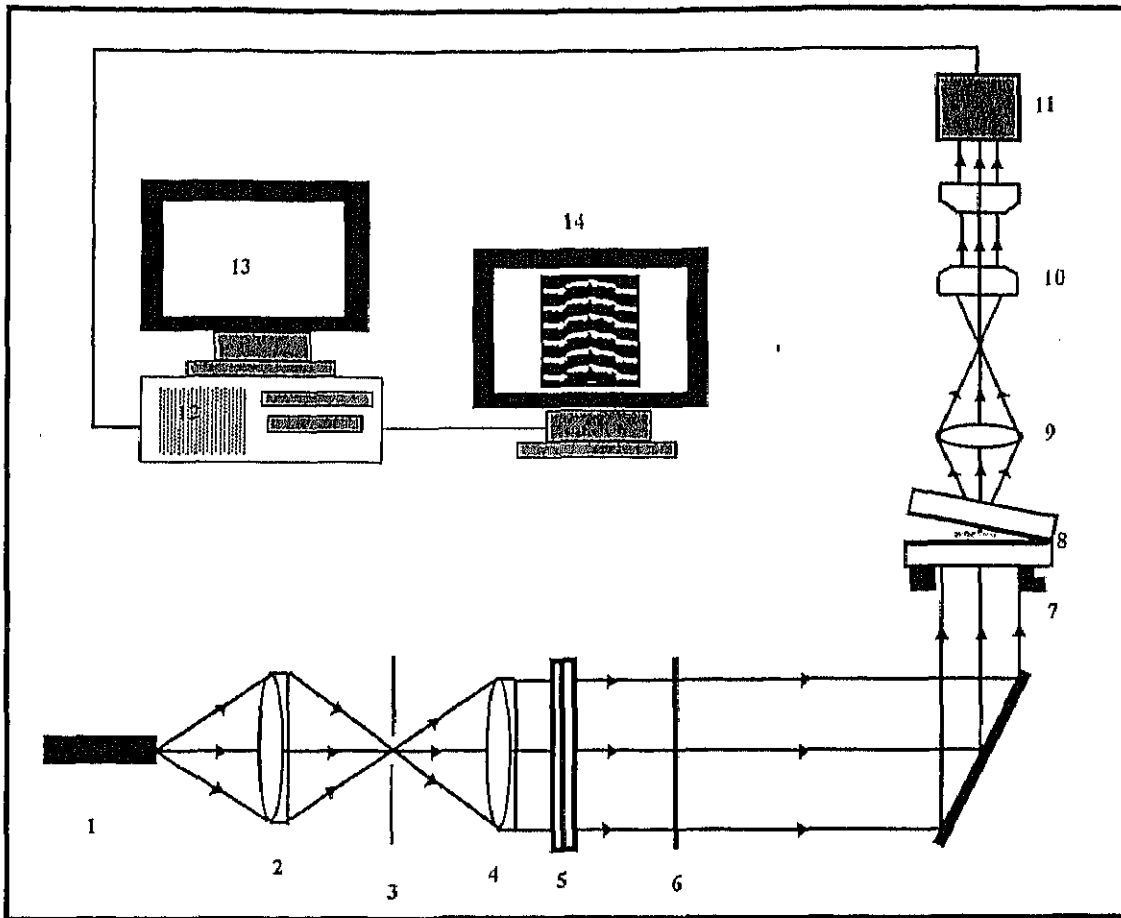


Figure 3 The optical setup for producing multiple-beam Fizeau fringes in transmission: 1, mercury lamp; 2, condenser lens; 3, iris diaphragm; 4, collimating lens; 5, polarizer; 6, monochromatic interference filter; 7, microscope stage; 8, silvered liquid wedge interferometer; 9, microscope objective; 10, microscope ocular; 11, CCD camera; 12, frame grabber; 13, graphic and text screen; 14, multisync monitor.

set to a bright value. On the other hand, if the derivative signs of the original fringe pattern of the points are negative, the points are set to a dark value, as shown in Figure 2(a,b). From this figure one can see that the boundaries of the binary fringes are exactly the centerlines of the original fringes without any deviation [Fig. 2(c)]. The derivative-sign binary fringe image is expressed as follows:

$$g(x, y) = \begin{cases} \text{bright color (say 255)} & \text{if } \Delta g(x, y) > 0 \\ \text{dark color (say 0)} & \text{if } \Delta g(x, y) < 0 \end{cases} \quad (6)$$

where

$$\Delta g(x, y) = g(x, y) - g(x + 1, y)$$

After constructing the derivative-sign binary image pattern it is easy to extract the fringe centerlines over the image field using the following equation:

$$g(x, y) = |g(x, y) - g(x - 1, y)| \quad (7)$$

EXPERIMENTAL

A schematic diagram representing the optical setup for producing multiple-beam Fizeau fringes is shown in Figure 3. The fringes are characterized by sharp bright fringe on a dark background. This system is reported elsewhere.⁹ The liquid

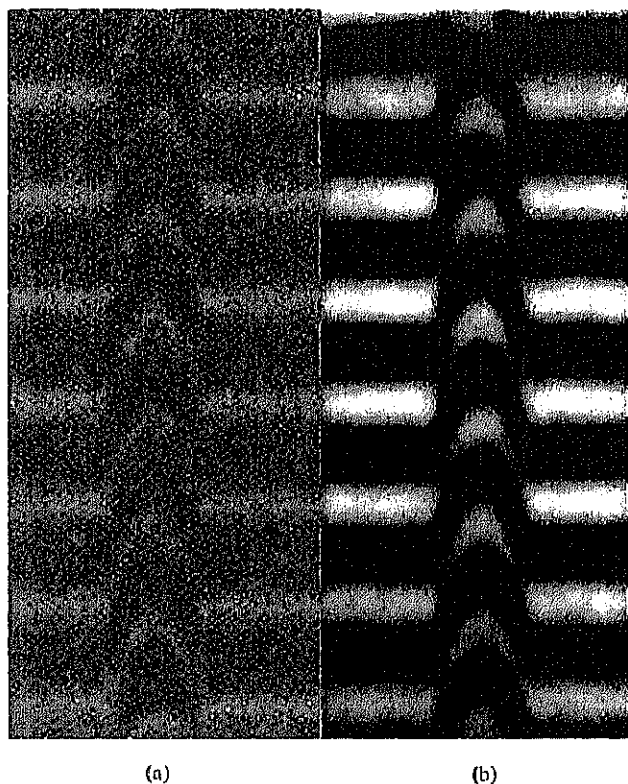


Figure 4 (a) The original microinterferogram of the polyethylene fiber with a draw ratio of 7.5 using monochromatic light vibrating parallel to the fiber axis and (b) the resultant noise-free normalized fringe pattern of the original.

wedge interferometer is adjusted in such a way that the fiber is exactly perpendicular to the interference fringes in the liquid region. The accuracy of the refractive index profile, and hence the structural parameter measurements, are affected by the deviation of the fiber and fringes from a right angle. Deviation from a right angle by 1° or less causes a negligible change in the measured quantities.⁵ The intensity of the multiple-beam Fizeau image is converted to an electric video signal and sampled to yield a digital picture made up of 512×512 sample points, each of which is quantized to 256 discrete gray levels. Using a 2-dimensional intensity sensor (Panasonic CCD microcamera attached directly to the microscope), the digital picture is stored in the memory of a digital frame grabber. The stored picture is transferred to a PC with a 500-MHz microprocessor and recorded on the mass storage device of a disk. A crosshair is used to adjust the fiber to be perpendicular to the fringes. A relay lens is inserted between the microscope and the CCD camera to sharpen the interferogram.

RESULTS AND DISCUSSION

Fringe Centerline Extraction

Two polyethylene fiber samples were used, which were drawn to different draw ratios (7.5 and 10). The draw ratio is the ratio of the fiber length after drawing to the original fiber length. Monochromatic light ($\lambda = 546.1$ nm) vibrating parallel and perpendicular to the fiber axis is used. Figure 4(a) is the original multiple-beam Fizeau fringe pattern of the polyethylene fiber with a draw ratio of 7.5. We applied the FT method to remove the pattern's noise and the result is shown in Figure 4(b).

To determine the contour line we must first determine the derivative binary fringe image of the pattern by using eq. (6). Thus, by determining the edges of the derivative binary fringe image, we can determine the contour line of the original bright fringe image. Figure 5(a) is the original fringe pattern produced by using polyethylene fiber with a draw ratio of 10 and light vibrating perpendicular to the fiber axis. Figure 5(b) is the contour line plotted inside the original pattern, while Figure 5(c) shows the contour line with a dark background. Figure 6(a–c) is the same as Figure 5(a–c) but using the light vibrating parallel to the fiber axis. Also, by using the real part of the IFT we could estimate another pattern, which coincides with the experimental pattern. Figure 7(a–c) shows the experimental pattern, the estimated pattern, and the derivative binary fringe

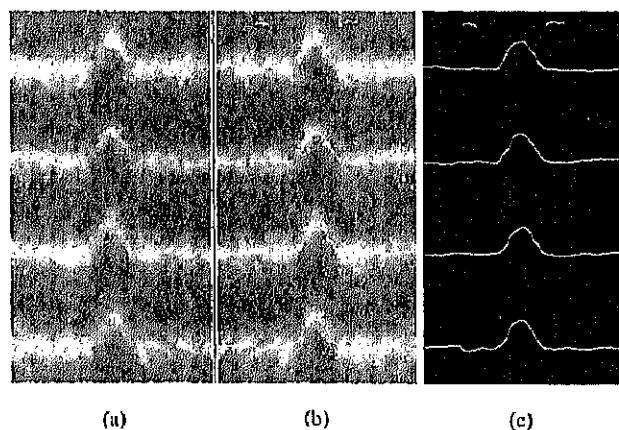


Figure 5 (a) A microinterferogram of the polyethylene fiber with a draw ratio of 10 using monochromatic light vibrating perpendicular to the fiber axis, (b) an extracted fringe contour line of the former shown on the background of the original pattern, and (c) the extracted fringe contour line in a dark background.

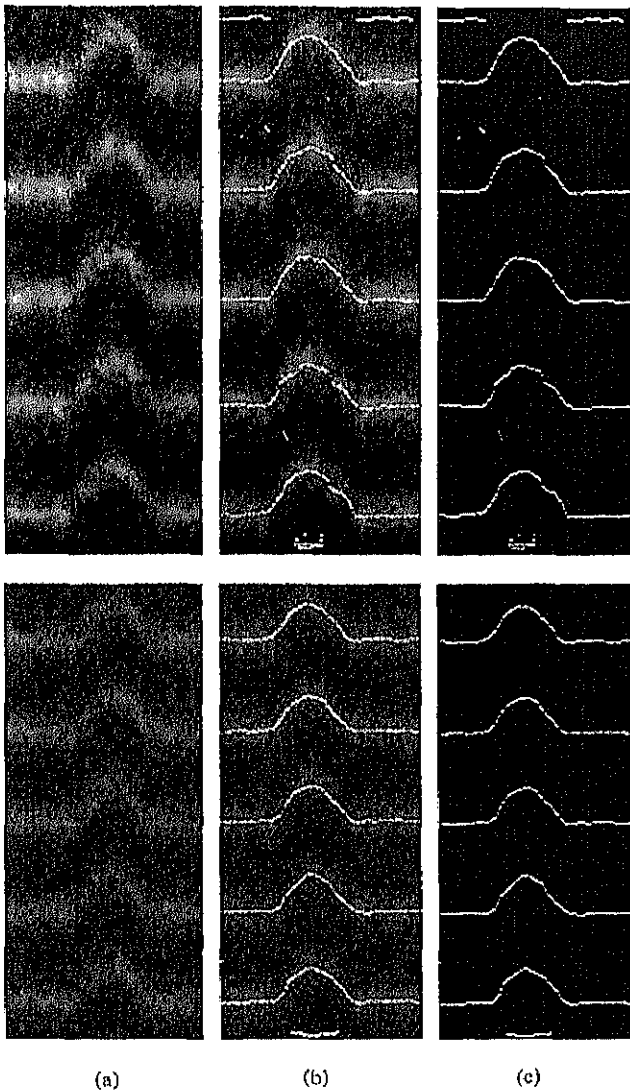


Figure 6 (a) A microinterferogram of the polyethylene fiber with a draw ratio of 10 using monochromatic light vibrating parallel to the fiber axis, (b) an extracted fringe contour line of the former shown on the background of the original pattern, and (c) the extracted fringe contour line in a dark background.

image of the estimated pattern. Figure 8(a) is the experimental image, Figure 8(b) is the contour line of this pattern, Figure 8(c) is the estimated pattern of Figure 8(a), and Figure 8(d) is the contour line of Figure 8(c). Observe that the contour line in Figure 8(d) is more stable than in Figure 8(b).

Refractive Index Profile Measurement

The refractive index profiles of the drawn fibers were obtained using the original and estimated

patterns. The monochromatic light had a 546.1-nm wavelength. The fringe patterns shown in Figure 8(a,c) were used to obtain the refractive index profile shown in Figure 9. The refractive index profiles shown in Figure 10 were calculated from the interferogram produced using polyethylene fiber with a draw ratio of 10 and monochromatic light vibrating perpendicular to fiber axis. The immersion liquid used had a refractive index of 1.5297, and the pixel size was found to be $0.87 \mu\text{m}$.

The pixel size plays an important role in the measurement accuracy, so the difference between the results of the methods applied in Figures 9 and 10 is due to the change in the pixel size. It is clear from Figures 9 and 10 that the refractive index profile is nearly flat. The relationship between the absolute difference in the average value of the refractive index of both methods and the pixel size is shown in Figure 11. From Figure 11 it is clear that with low pixel size there is little difference in the results of both methods, so we recommend use of this method with low pixel size. Considering the affect of the pixel size in the measurement accuracy, the microinterferogram shown in Figure 6(a, upper) has a pixel size of $0.625 \mu\text{m}$. The refractive index profile given in Figure 12 is calculated from this microinterferogram and its estimated pattern. It is clear that there is only a small error in the measurement of the refractive index for both methods, and the two curves in Figure 12 coincide with each other and tend to be one curve.

The fringe pattern shown in Figure 7(a) is so poor that it was not possible to automatically

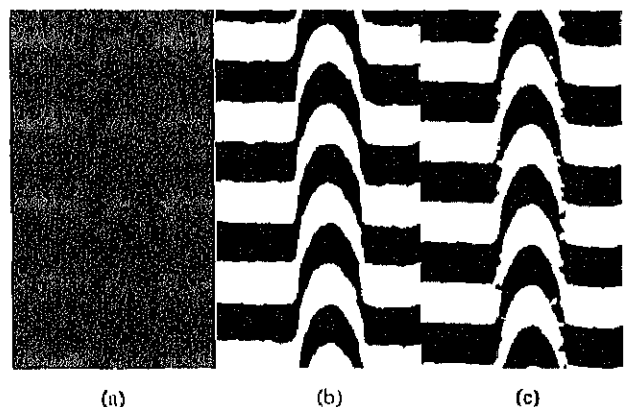


Figure 7 (a) The original pattern, (b) the estimated pattern produced by using the real part of the inverse Fourier transform of the original, and (c) the derivative binary fringe image of the estimated pattern.

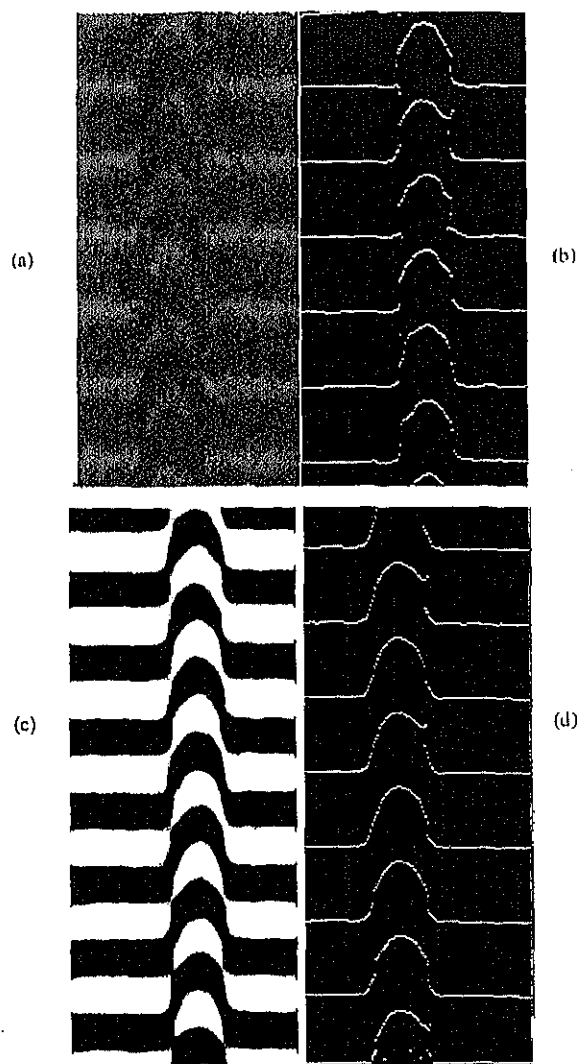


Figure 8 (a) The original pattern, (b) the contour line of the fringe pattern (original), (c) the estimated pattern produced using the real part of the inverse Fourier transform of the original, and (d) the contour line of the fringe pattern (estimated).

determine its contour line, so we manually calculated the refractive index. However, its estimated fringes were used to automatically calculate the refractive index profile as shown in Figure 13. The results show good agreement, which encourages use of the suggested method of estimated fringes to determine the refractive index profile of the fiber.

CONCLUSIONS

Compared with conventional methods, the FT method has the advantage of higher accuracy.²⁹ It

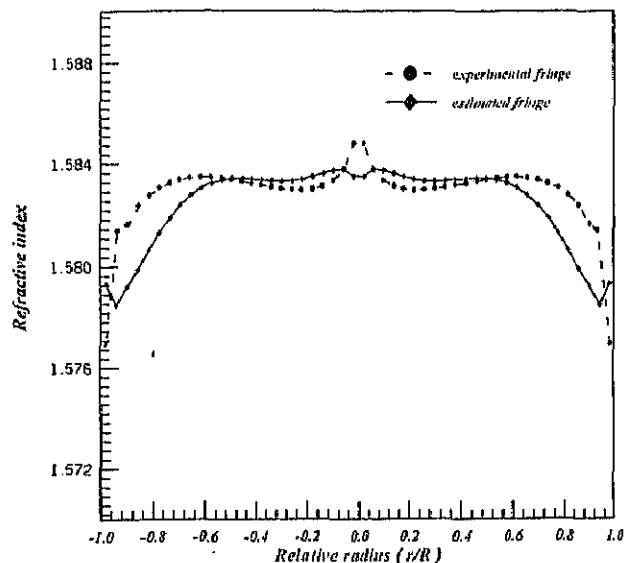


Figure 9 The refractive index profile of the polyethylene fiber with a draw ratio of 7.5 using experimental and estimated patterns. Monochromatic light vibrating parallel to the fiber axis was used. The pixel size is $1.32 \mu\text{m}$, and the immersion liquid has a refractive index of 1.5787.

could be used to enhance and analyze multiple-beam Fizeau fringes. Fully automated determination of the contour line is possible, whatever the

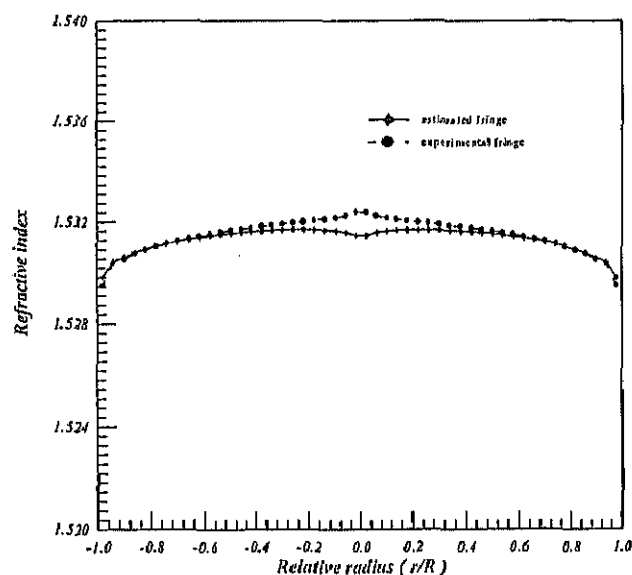


Figure 10 The refractive index profile of the polyethylene fiber with a draw ratio of 10 using experimental and estimated patterns. The monochromatic light vibrates perpendicular to the fiber axis. The pixel size is $0.87 \mu\text{m}$, and the immersion liquid has a refractive index of 1.5297.

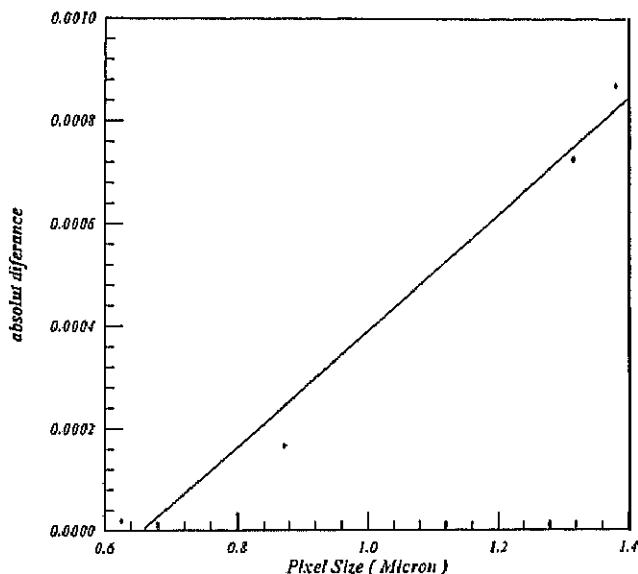


Figure 11 The relationship between the pixel size and the absolute difference of the average values of the refractive index measured by the experimental and estimated patterns.

quality of the interference image being used. The suggested methods described in this article are particularly suitable for applications involving

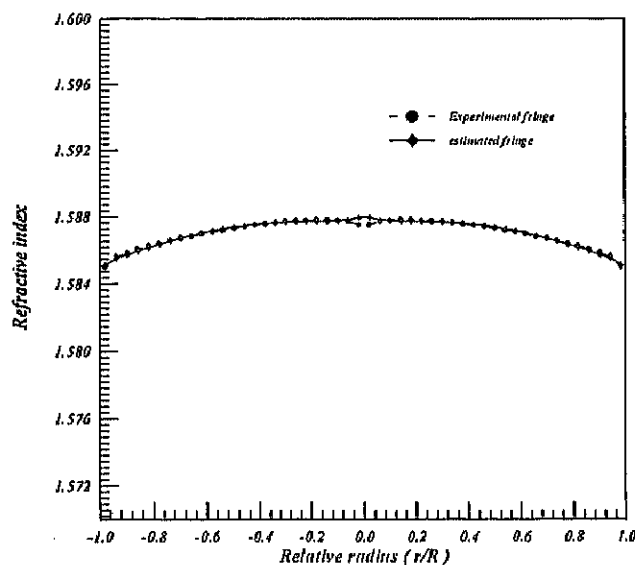


Figure 12 The relationship between the pixel size and the absolute difference of the average values of the refractive index measured by the experimental and estimated patterns. Monochromatic light vibrates parallel to the fiber axis. The pixel size is small enough ($0.625 \mu\text{m}$), and the immersion liquid has a refractive index of 1.5849.

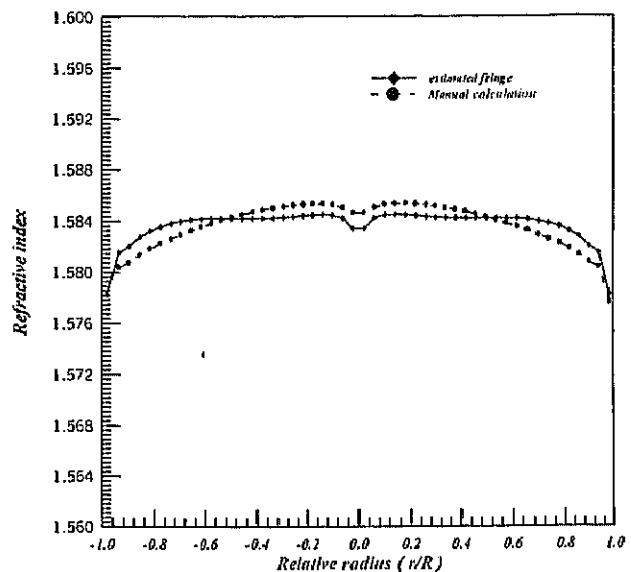


Figure 13 The refractive index profile of the polyethylene fiber with a draw ratio of 7.5 using experimental and estimated patterns. Monochromatic light vibrating parallel to the fiber axis is used. The pixel size is $0.8358 \mu\text{m}$, and the immersion liquid has a refractive index of 1.5787.

high quality and low quality patterns. On the other hand, we can estimate a new pattern, which coincides with the experimental pattern, and use it to calculate the refractive index profile. The highest accuracy of the refractive index profile was obtained with low pixel size.

REFERENCES

1. Zanger, H.; Zanger, C. *Fiber Optics Communications and Other Applications*; Maxwell Macmillan: New York, 1991.
2. Faust, R. C. *Physical Methods of Investigation Textiles*; Textile Book Publishers Inc.: New York, 1959.
3. Sounders, M. J.; Gardner, W. B. *Appl Opt* 1977, 16, 2368.
4. Sochacki, J. *Appl Opt* 1986, 25, 3473.
5. Hamza, A. A.; Mabrouk, M. A. *J Mod Opt* 1991, 38, 97.
6. Barakat, N.; Hamza, A. A.; Gonied, A. S. *Appl Opt* 1985, 24, 4383.
7. Hamza, A. A.; Sokkar, T. Z. N.; Mabrouk, M. A.; Ghandar, A. M.; Ramadan, W. A. *Pure Appl Opt* 1995, 4, 161.
8. Hamza, A. A.; Sokkar, T. Z. N.; Mabrouk, M. A.; El-Morsy, M. A. *J Appl Polym Sci* 2000, 77, 3099.
9. Barakat, N.; Hamza, A. A. *Interferometry of Fibrous Materials*; Adam-Hilger: Bristol, U.K., 1990.

10. Okoski, T. *Optical Fibres*; Harcourt Brace Jovanovich: New York, 1982.
11. Mabrouk, M. A.; El-Bawab, H. F. *Pure Appl Opt* 1997, 6, 247.
12. Mabrouk, M. A.; Shams-Eldin, M. A. *Pure Appl Opt* 1996, 5, 929.
13. Yatagai, T.; Nakadate, S.; Idesawa, M.; Saito, H. *Opt Eng* 1982, 21, 432.
14. Chen, T. Y.; Taylor, C. E. *Exp Mech* 1989, 29, 323.
15. Ramesh, K.; Singh, R. K. *Electron Imag* 1995, 4, 71.
16. Yao, J. Y. *Exp Mech* 1990, 30, 264.
17. Eichhorn, N.; Osten, W. *J Mod Opt* 1988, 35, 1717.
18. Yu, Q. Y.; Liu, X. L.; Andresen, K. *Appl Opt* 1994, 33, 3705.
19. Yu, Q. Y.; Liu, X. L.; Sun, X. *Appl Opt* 1998, 37, 4504.
20. Takeda, M.; Ina, H.; Kobayashi, S. *J Opt Soc Am* 1982, 72, 156.
21. Takeda, M.; Mutoh, K. *Appl Opt* 1983, 22, 3977.
22. Burton, D. R.; Lalor, M. *J Proc SPIE* 1988, 1010, 17.
23. Bone, D. J. *Appl Opt* 1991, 30, 3627.
24. Nugent, K. A. *Appl Opt* 1985, 24, 3101.
25. Lai, G.; Yatagai, T. *Appl Opt* 1994, 33, 5935.
26. Arevalillo, M.; Burton, D. R.; Lalor, M. J. *Opt Laser Eng* 1999, 31, 135.
27. Green, R. J.; Walker, J. G.; Robinson, D. W. *Opt Laser Eng* 1988, 8, 29.
28. Nakadate, S.; Yatagai, T.; Saito, H. *Appl Opt* 1983, 22, 237.
29. Liu, J. B.; Ronney, P. D. *Appl Opt* 1997, 36, 6231.

Automatic refractive index profiling of fibers by phase analysis method using Fourier transform

M.A. El-Morsy^{a,*}, T. Yatagai^a, A.A. Hamza^b, M.A. Mabrouk^c,
T.Z.N. Sokkar^b

^a*Institute of Applied Physics, Yatagai Laboratory, University of Tsukuba, Tsukuba, Ibaraki 305-5873, Japan*

^b*Physics Department, Faculty of Science, University of Mansoura, Mansoura, Egypt*

^c*Physics Department, Faculty of Science, Demietta, University of Mansoura, Demietta, Egypt*

Received 1 May 2001; received in revised form 1 December 2001; accepted 1 January 2002

Abstract

Automatic fringe pattern analysis is a powerful and inexpensive digital image-processing technique. It is used to analyze the fringe pattern obtained by different optical techniques, such as multiple-beam Fizeau fringes. To perform accurate and fast automatic measurement of fiber refractive index profile, phase analysis method has been used with the Fourier transform technique. In this paper, the refractive index profiles of polyethylene fibers with different draw ratios are presented by two methods, fringe shift method and phase analysis method. A comparison between the results obtained is presented. © 2002 Elsevier Science Ltd. All rights reserved.

Keywords: Automatic fringe analysis; Fourier transform; Phase measurement; Multiple-beam Fizeau fringes; Refractive index profile; Polyethylene fiber

1. Introduction

In the present decade, much progress has been made in the field of optical measurement because of several major advances in its related technologies. Optical measurement is based on the wave characteristics of light when it reflects from or transmits through an object. Light transmission properties through a fiber depend mainly on its refractive index profile and material dispersion. The refractive index

*Corresponding author. Fax: +81-298-53-5305.

E-mail addresses: elmorsy@optlab2.bk.tsukuba.ac.jp, elmorsym@yahoo.com (M.A. El-Morsy).

profile of optical or textile fiber is important not only in assessing the performance of the fiber in a given system but also it helps in fiber fabrication to improve its products. Therefore, there is an increasing need for fast and accurate measurement of refractive index profile of fibers because it provides information for the correlation between their structure and the other properties.

Many different techniques were applied to determine the refractive index profile of fibers. One of the most sensitive and non-destructive technique, used to obtain this information, is multiple-beam Fizeau fringe system. So, this technique has been successfully used to investigate textile and optical fibers [1–6].

In practice, the fiber samples are immersed in a silvered liquid wedge interferometer [3], which act as phase objects displacing the normally straight parallel fringes of the multiple-beam Fizeau fringe interferometer to the fiber region. This fringe displacement or *shift* is proportional to the index difference Δn between the fiber refractive index and the immersion liquid. The methods in which a matching immersion liquid is used to give good results of fiber refractive index profile, especially when both liquid and fiber cladding have refractive indices close to each other.

The principle problem in accurately measuring the refractive index using multiple-beam Fizeau fringe system, is how to determine the contour line of the fringe pattern for; (a) interference fringe shift [3,7] or (b) the area enclosed under the fringe shift, and interfringe spacing. The present paper focuses on the refractive index profile measurement using the phase shift instead of fringe shift (or) the area under fringe shift and interfringe spacing.

Image-processing techniques were used to analyze the fringe pattern to perform automated, high-speed, and accurate analysis [8–10]. To analyze interference fringes accurately, the phase shift and Fourier transform measurement techniques were developed [11–17]. These techniques can be essentially classified into two basic types: the phase shifting and the Fourier transform types. Phase shifting techniques usually require at least three phase shifted interference fringe patterns. On the other hand, Fourier transform method usually requires only one interference fringe pattern for extracting phase information. This technique has been applied to various kinds of interferometric techniques.

2. Theory

2.1. Optical path difference

To produce multiple-beam Fizeau fringes in transmission, a parallel beam of plane polarized light illuminates a wedge interferometer placed on a microscope stage with normal incidence. This wedge interferometer consists of two circular optical flats. The inner surface of each flat is coated with a highly reflecting (75%) and partially transmitting (22%) silver layer. Both the gap thickness and the wedge angle are selected to form the sharpest fringes at right angles to the edge of the wedge. The fiber in the matching liquid acts as a phase object. The amount of the phase shift

depends upon the values of refractive indices of the fiber and the immersion liquid used. The phase difference is given by

$$\phi = \frac{2\pi}{\lambda} m\Delta, \quad (1)$$

where m is an integer number equal to 1 in the case of two beam interference and 2 in the case of multiple-beam interference, λ is the wavelength of light used, Δ is the optical path difference. An accurate mathematical expression for the optical path difference (OPD) was given by Hamza et al. [5] in which they considered the refraction of the beam through the fiber due to refractive index change along its radius. Also, they considered that the fiber is assumed to be divided into N circular zones. For large number of layers, each layer can be considered to have a constant refractive index. A general expression is used to calculate the Δ_Q of the Q th layer in the fiber region, in case of multiple-beam Fizeau fringes as follows:

$$\begin{aligned} \Delta_Q = & \sum_{j=1}^{Q-1} 2n_j \left\{ \sqrt{(R - (j-1)a)^2 - (d_Q n_0/n_j)^2} \right. \\ & \left. - \sqrt{(R - ja)^2 - (d_Q n_0/n_j)^2} \right\} \\ & + 2n_Q \sqrt{(R - (Q-1)a)^2 - (d_Q n_0/n_Q)^2} \\ & - n_0 \left\{ \sqrt{R^2 - d_Q^2} + \sqrt{R^2 - X_Q^2} \right\}, \end{aligned} \quad (2)$$

where R is the fiber radius, a is the layer thickness ($a = R/N$), $n_0 = n_L$ is the immersion liquid refractive index, X_Q and d_Q are the emerged and incident rays distances from the fiber center, respectively, where

$$d_Q = \frac{n_Q(R - (Q-1/2)a)}{n_0}.$$

And considering that the phase difference is given by

$$\phi = \phi(R) - \phi_0$$

$\phi(R)$ is the phase shift due to the fiber and ϕ_0 is the phase due to the immersion liquid. The value of ϕ_0 must be constant. Because the interferogram has a noise this value is not exactly constant but we can say it is nearly constant so we calculate the main value of ϕ_0 .

$$\frac{\lambda \phi_Q}{4\pi} = \Delta_Q$$

$$\begin{aligned}
&= \left[\sum_{j=1}^{Q-1} 2n_j \left\{ \sqrt{(R - (j-1)a)^2 - (d_Q n_0 / n_j)^2} \right. \right. \\
&\quad \left. \left. - \sqrt{(R - ja)^2 - (d_Q n_0 / n_j)^2} \right\} \right. \\
&\quad \left. + 2n_Q \sqrt{(R - (Q-1)a)^2 - (d_Q n_0 / n_j)^2} \right. \\
&\quad \left. - n_0 \left(\sqrt{R^2 - d_Q^2} + \sqrt{R^2 - X_Q^2} \right) \right].
\end{aligned}$$

2.2. Phase measurement

Mapping the phase of the fringes displayed on an interferogram is an important problem in many areas of optical measurement. In the 1970s Bruning et al. [18] introduced to interferometry a phase-detection technique for testing optical

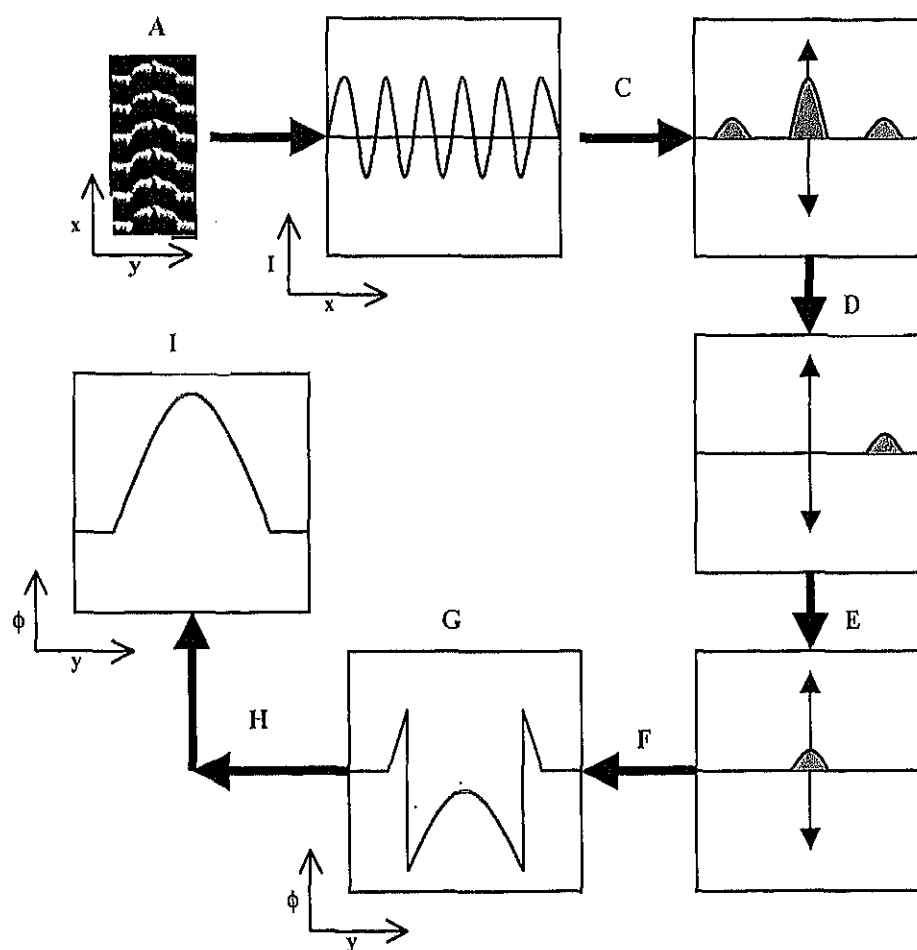


Fig. 1. Fourier transform process; A—original pattern; B—1-D intensity distribution; C—FFT process; D—filter process; E—shifting process; F—IFFT process; G—wrapped phase obtained; H—unwrapped phase process; I—unwrapped phase obtained.

components that uses a solid-state detector. In this method, an interference pattern was phase shifted and the digitized intensity values were then correlated with sines and cosines to determine the optical phase. This method requires at least three phase-shifted interferograms. In 1982 Takeda et al. [16] proposed a novel method of phase analysis using Fourier transform. The phase can be retrieved from a single interferogram by using this method. This technique has been used and modified by several authors [15,19,20]. This technique is summarized as follows.

Generally, the intensity distributions in such interference fringe pattern can be written as

$$g(x, y) = a(x, y) + b(x, y)\cos(2\pi f_0 x + \phi(x, y)), \quad (4)$$

where $a(x, y)$ represents the background illuminations of the intensity distribution $g(x, y)$, $b(x, y)$ describes the amplitude of the corresponding interference fringe, f_0 is the carrier frequency, $\phi(x, y)$ is the phase of the object that we have to analyze at any point (x, y) on the interferogram. In most cases $a(x, y)$, $b(x, y)$, and $\phi(x, y)$ are very slowly varying functions compared with the variation introduced by the spatial

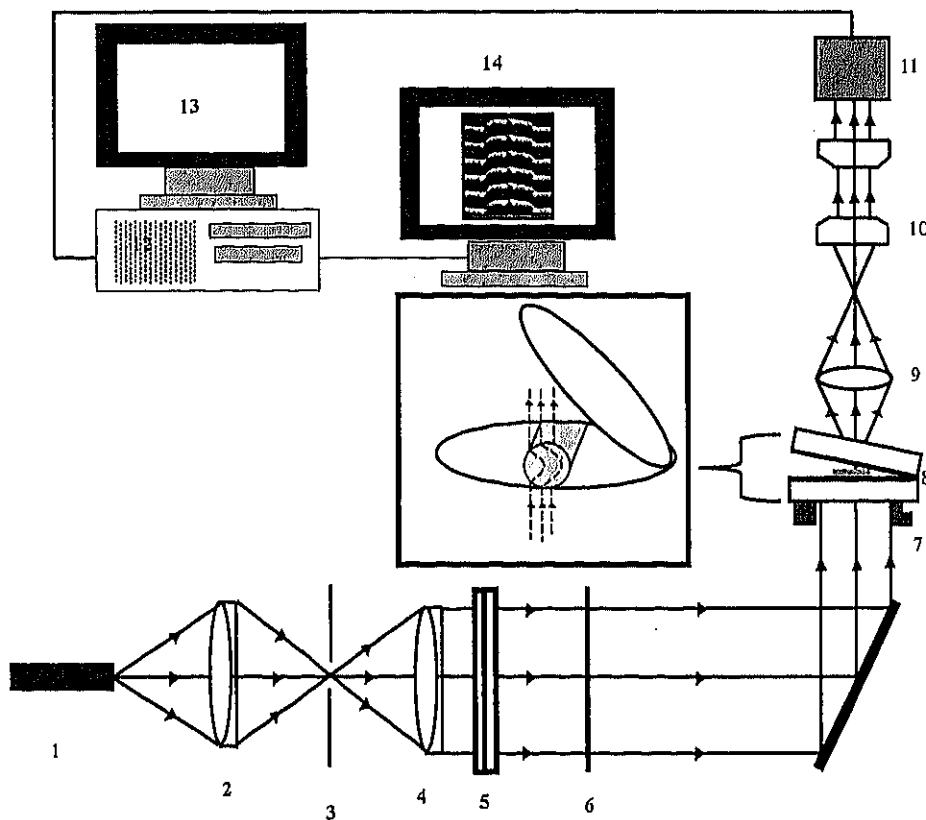


Fig. 2. The optical setup for producing multiple-beam Fizeau fringes in transmission: 1—Mercury lamp; 2—condenser lens; 3—Iris diaphragm; 4—Collimating lens; 5—Polarizer; 6—Monochromatic interference filter; 7—Microscope stage; 8—Silvered liquid wedge interferometer; 9—Microscope objective; 10—Microscope ocular; 11—CCD camera; 12—Frame grabber; 13—Graphic and text screen; 14—Multisync monitor.

carrier frequency f_0 . This equation can be rewritten as

$$g(x, y) = a(x, y) + c(x, y)\exp(i2\pi f_0 x) + c^*(x, y)\exp(-i2\pi f_0 x), \quad (5)$$

where

$$c(x, y) = \frac{1}{2} b(x, y)\exp(i\phi(x, y)) \quad (6)$$

and $c^*(x, y)$ denotes complex conjugation of $c(x, y)$.

Applying Fourier transform (FT) algorithm, we compute the one-dimension (1-D) Fourier transform of Eq. (5) for the variable x only, with y being fixed.

$$G(f, y) = A(f, y) + C(f - f_0, y) + C^*(f + f_0, y), \quad (7)$$

where the capital letters denote Fourier spectra, f is the variable in spatial frequency space and $C(f - f_0, y)$ is the FT of $c(x, y)$ with respect to x . From Eq. (7) one can notice that, the FT of the fringe pattern exhibit three distinct peaks. The Fourier transform of the term $A(f, y)$ is placed in the center of the spectrum and represents the zero frequency (or DC). And the Fourier transforms of $C(f - f_0, y)$ and $C^*(f + f_0, y)$ then will be symmetric with respect to the center and placed at a distance that is determined by f_0 . We make use of either of the two peaks spectra on the carrier, say

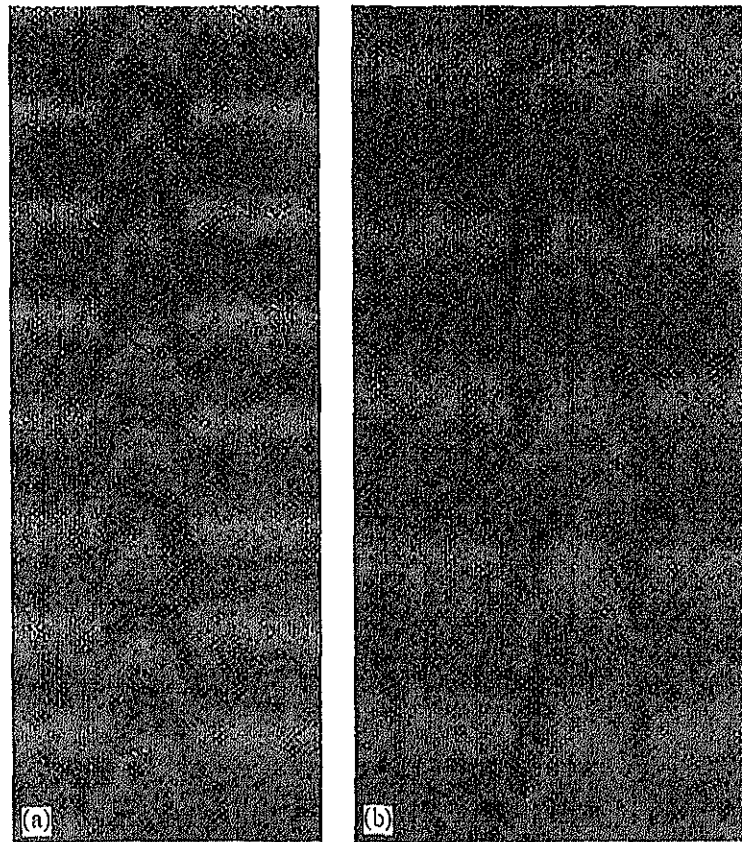


Fig. 3. Microinterferogram of polyethylene fiber with the draw ratio 7.5 using monochromatic light vibrating parallel to the fiber axis, immersion liquid used is 1.5787 (A) pixel size is 1.316614 μm , (B) pixel size is 0.8665226 μm .

$C(f - f_0, y)$. In other words, the unwanted peaks have been filtered out in this step. After $C(f - f_0, y)$ is shifted a distance of f_0 toward the original in the frequency domain, we compute the inverse Fourier transform (IFT) of $C(f - f_0, y)$ with respect to f then the term $c(x, y)$ itself will be obtained. Then we calculate a complex logarithm of Eq. (6)

$$\log[c(x, y)] = \log\left[\frac{1}{2} b(x, y)\right] + i\phi(x, y).$$

From this equation it is easy to obtain the phase. In most cases, a computer-generated function subroutine gives a principal value ranging from $-\pi$ to π . So, the phase map obtained is wrapped in the range between $-\pi$ and π , and the phase unwrapping procedure is generally required to produce a continuous phase distribution. The relation between the wrapped and the unwrapped phase can be stated as

$$\begin{aligned} \phi(x_i, y_j) &= \phi_w(x_i, y_j) + 2\pi m(x_i, y_j), \\ 1 \leq i \leq N, \quad 1 \leq j \leq M, \end{aligned} \quad (8)$$

where $\phi_w(x, y)$ is the wrapped phase, $\phi(x, y)$ is the unwrapped phase, and $m(x, y)$ is an integer-valued number called the field number. The unwrapping problem is trivial for phase maps calculated from good quality fringe data when the following two conditions are satisfied [21]:

- (1) The signal is free of noise.
- (2) The Nyquist condition is not violated, which means that the absolute value of the phase difference between any two consecutive phase samples (pixels) is $< \pi$.

The whole Fourier transform analysis process is illustrated in Fig. 1.

3. Experimental setup

Schematic diagram represents the optical setup for producing multiple-beam Fizeau fringes in transmission is shown in Fig. 2. The fringes are characterized by sharp bright fringe on a dark background. A parallel beam of monochromatic light falls on the plane-mirror of the microscope that reflects the light in a direction perpendicular to the wedge interferometer. The wedge interferometer is adjusted in such a way that the fiber is exactly perpendicular to the interference fringes in the liquid region. The accuracy of the refractive index profile and hence the structural parameters measurement are affected by the deviation of the fiber and fringes from the right angle. Deviation from right angle by one degree or less causes a negligible change in the measured quantities. The intensity of the multiple-beam Fizeau image is converted to an electric video signal and sampled to yield a digital picture made up of 512×512 sample points, each of which is quantized to 256 discrete gray levels. Using two-dimensional intensity sensor (Panasonic CCD micro-camera attached directly to the microscope), the digitized picture is stored in a digital frame grabber memory. The stored picture transferred to PC with microprocessor 500 MHz and

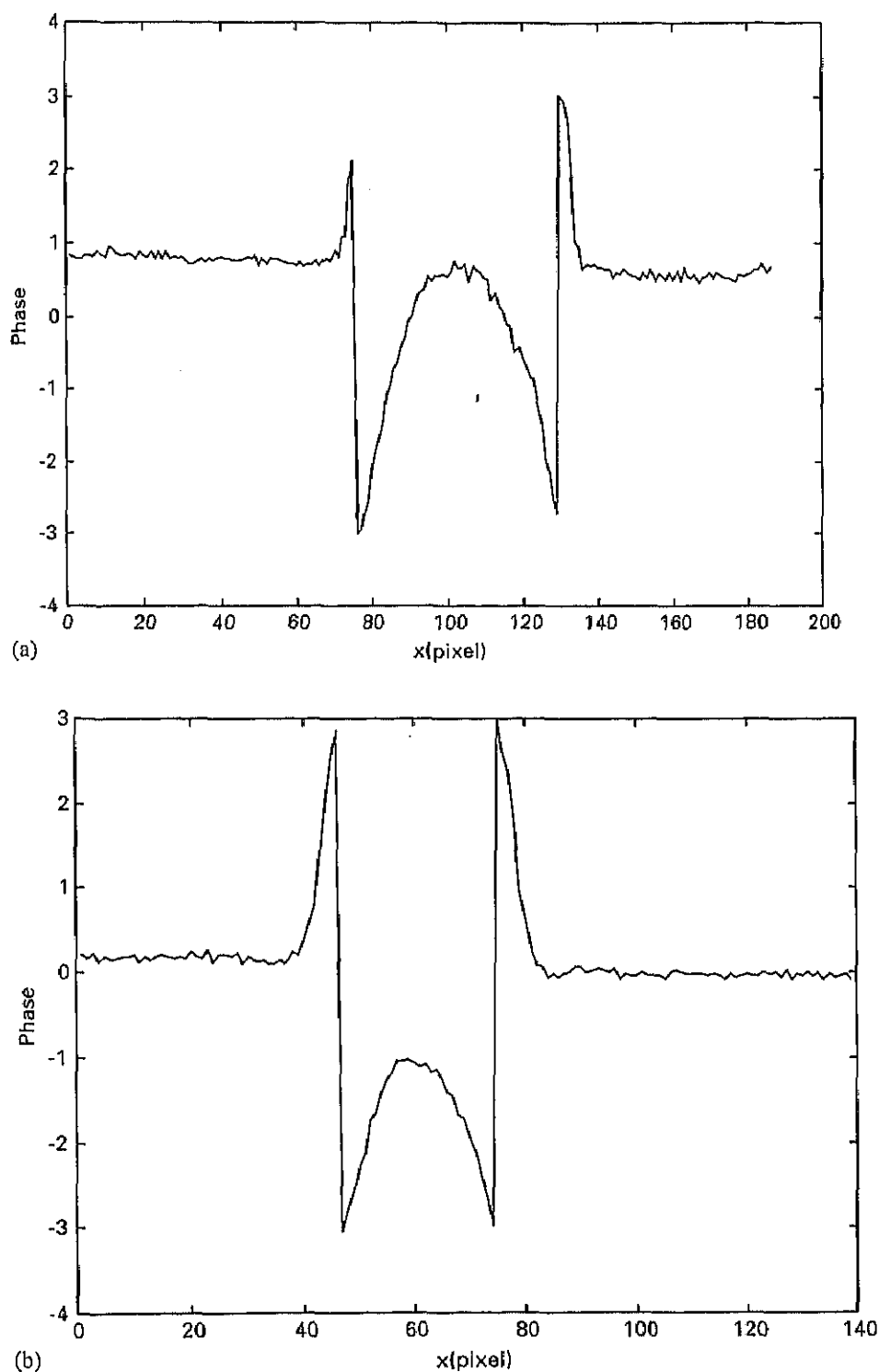


Fig. 4. The 1-D wrapped phase profile (A) of Fig. 3A, (B) of Fig. 3B.

recorded on the mass storage device of a disk. A cross hair is used to adjust the fiber to be perpendicular to the fringes. A relay lens is inserted between the microscope and the CCD camera to sharpen the interferogram.

4. Result and discussion

Mapping the phase and refractive index profiles of polyethylene fiber, which was drawn to different draw ratios (7.5 and 10), were obtained automatically. The draw

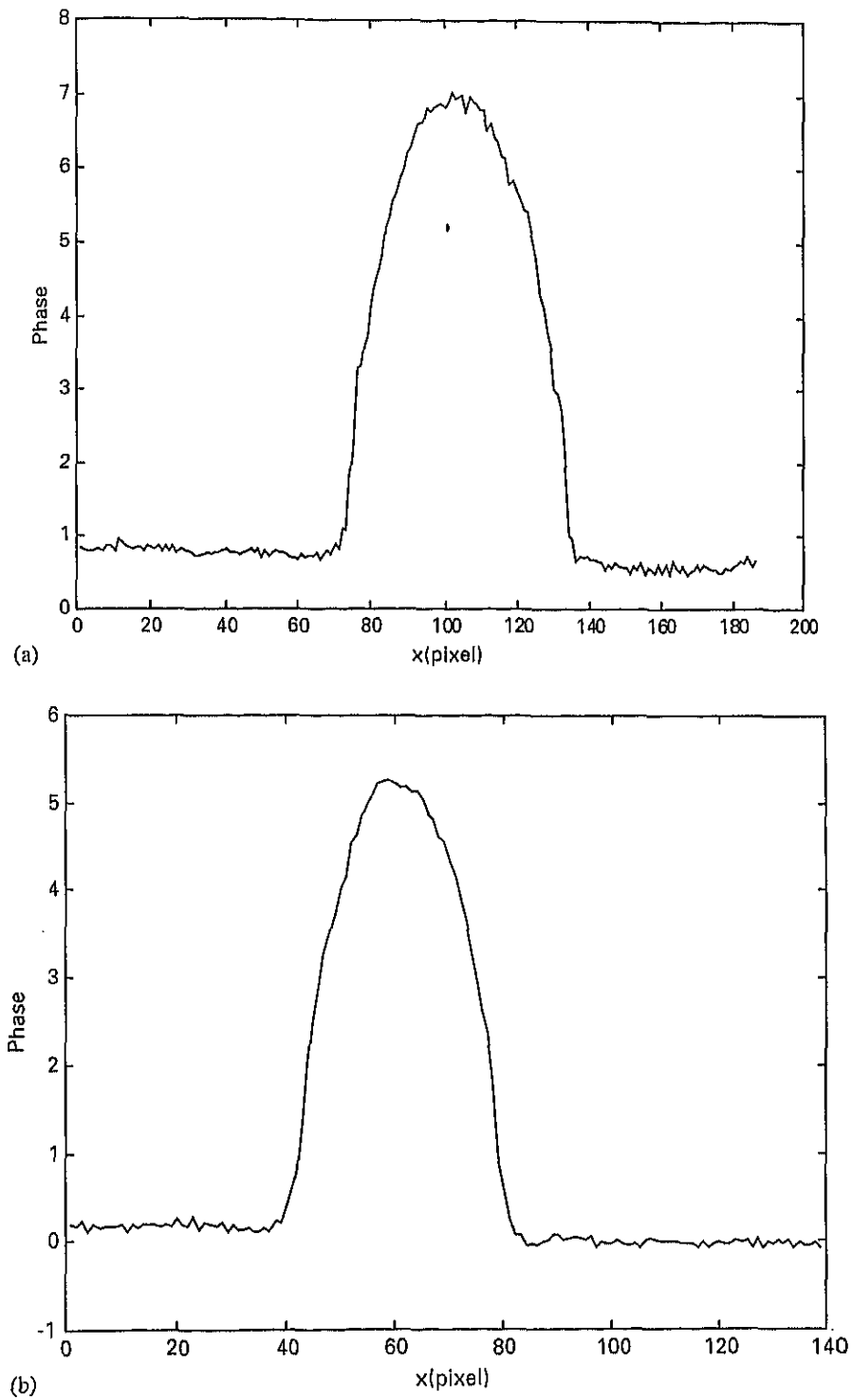


Fig. 5. The 1-D unwrapped phase profile (A) of Fig. 3A, (B) of Fig. 3B.

ratio is the ratio of the fiber length after drawing to the fiber original length. Monochromatic light of wavelength 546.1 nm vibrating parallel to the fiber axis is used. Fig. 3A shows the original interferogram of multiple-beam Fizeau fringe pattern of polyethylene fiber with the draw ratio 7.5 when using immersion liquid of refractive index 1.5787 and the pixel size is 1.32 μm . Fig. 3B shows the same but with the pixel size 0.87 μm . FT of the fringe pattern was taken to the interferograms which

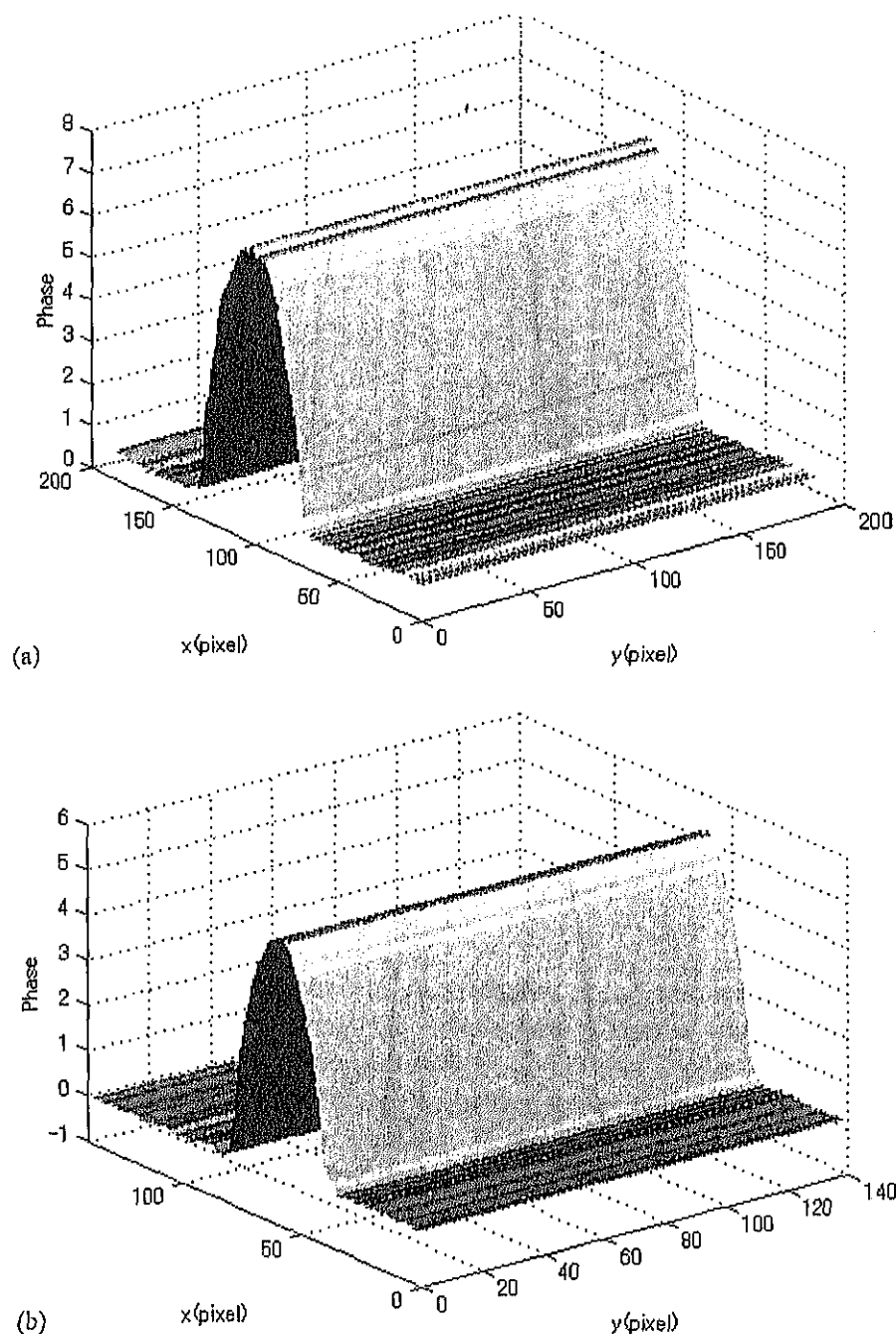


Fig. 6. Plot of the 2-D unwrapped continuous phase distribution (A) of Fig. 3A, (B) of Fig. 3B.

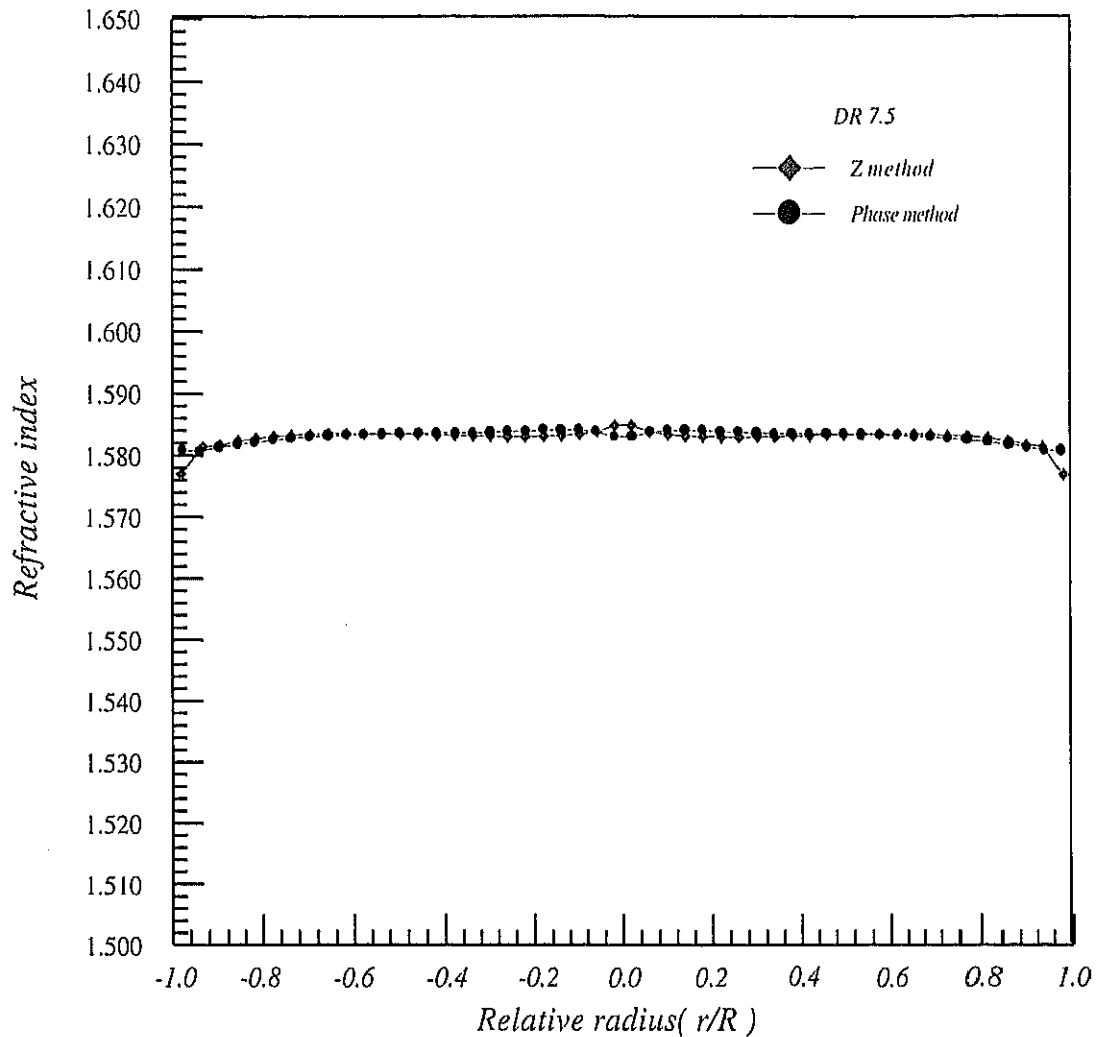


Fig. 7. Refractive index profile of polyethylene fiber with the draw ratio 7.5 using phase method and Z-method. Monochromatic light vibrating parallel to the fiber axis is used and the pixel size is found to be 1.31661 μm and the immersion liquid used is 1.5787.

are shown in Figs. 3A and B to obtain the wrapped phase, shown in Figs. 4A and B, respectively. Figs. 5A and B show the unwrapped phase in one dimension (1-D) while the unwrapped phase in two dimensions (2-D) was shown in Figs. 6A and B. Eq. (3) was used with software prepared by us to determine the refractive index along the fiber radius (refractive index profile). These results were compared with the refractive index profiles, which are obtained using fringe shift method (Z-method), shown in Figs. 7 and 8.

Fig. 9 shows the original interferogram of polyethylene fiber with the draw ratio 10 immersed in a liquid of refractive index 1.5849 and the pixel size is found to be 0.625 μm . The 1-D and the 2-D unwrapped phase were shown in Figs. 10 and 11, respectively. Fig. 12 shows the refractive index profile compared with that calculated

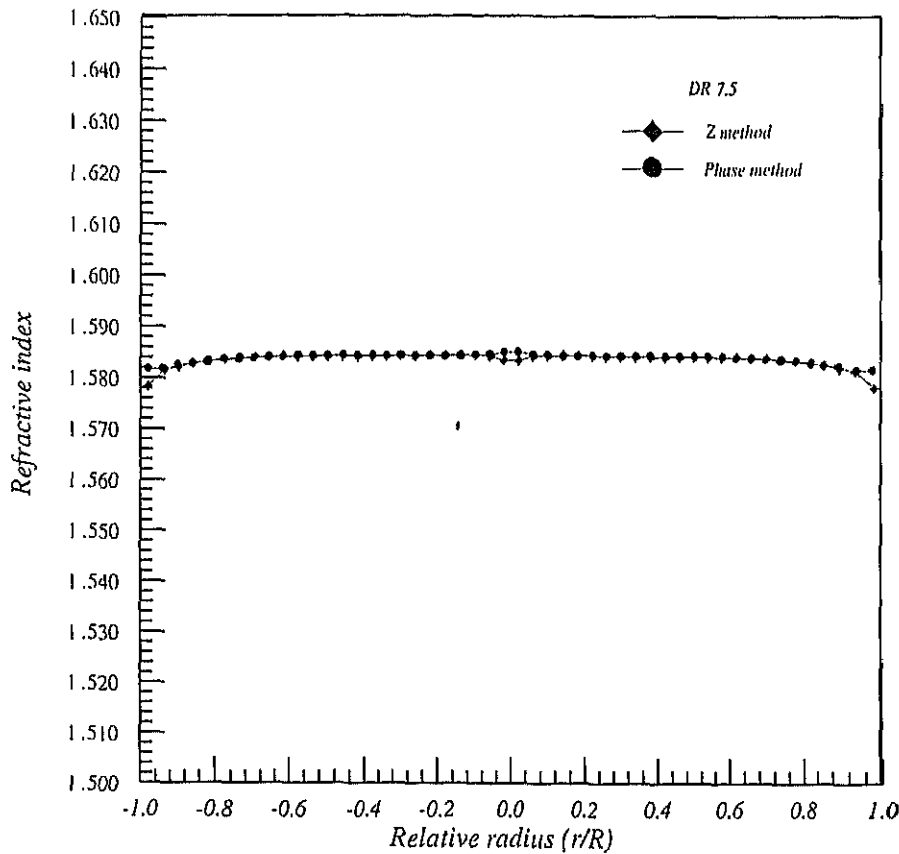


Fig. 8. Refractive index profile of polyethylene fiber with the draw ratio 7.5 using phase method and Z-method. Monochromatic light vibrating parallel to the fiber axis is used and the pixel size is found to be $0.8665\ \mu\text{m}$ and the immersion liquid used is 1.5787.

using Z-method. It is clear that, when the immersion liquid and fiber refractive indices are close to each other, a small error in the measurements of both method (phase method and Z-method) is obtained and the two curves coincide with each other and tend to be one curve.

In fact, the fibers used in this study have nearly constant refractive index profile. Referring to Figs. 3, 7, 8 and 12 one can easily notice that: (a) the applied phase with FT method gives a stable profile which is more reliable than that uses the fringe shift method, (b) as the difference in fiber and immersion liquid refractive indices increases the errors in the measurement increases, but still the phase with Fourier method has a good presentation of refractive index profile, (c) the smaller value of pixel size the more accurate are the obtained results.

Table 1 lists a statistical comparison between phase method and Z-method. From which, it can be seen that the refractive index profile measured using phase method is more accurate than that obtained by Z-method. Also, it shows that at low pixel size a small error in the results of both method is obtained.

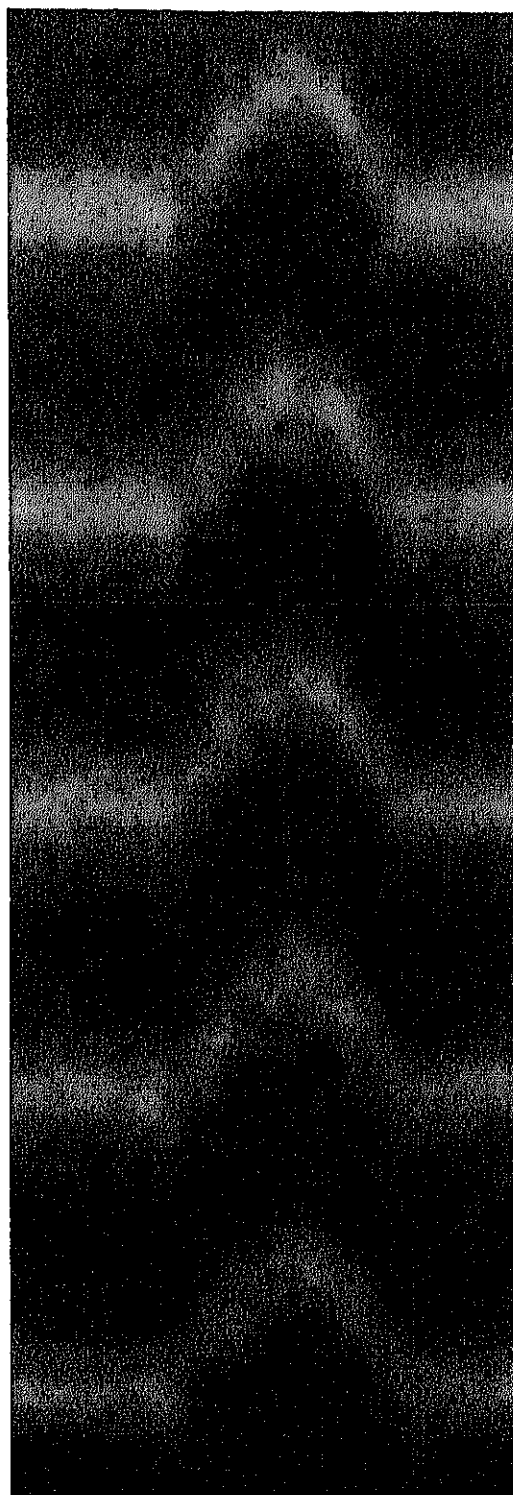


Fig. 9. Microinterferogram of polyethylene fiber with the draw ratio 10 using monochromatic light vibrating parallel to the fiber axis, immersion liquid used is 1.5849, and pixel size is $0.625\text{ }\mu\text{m}$.

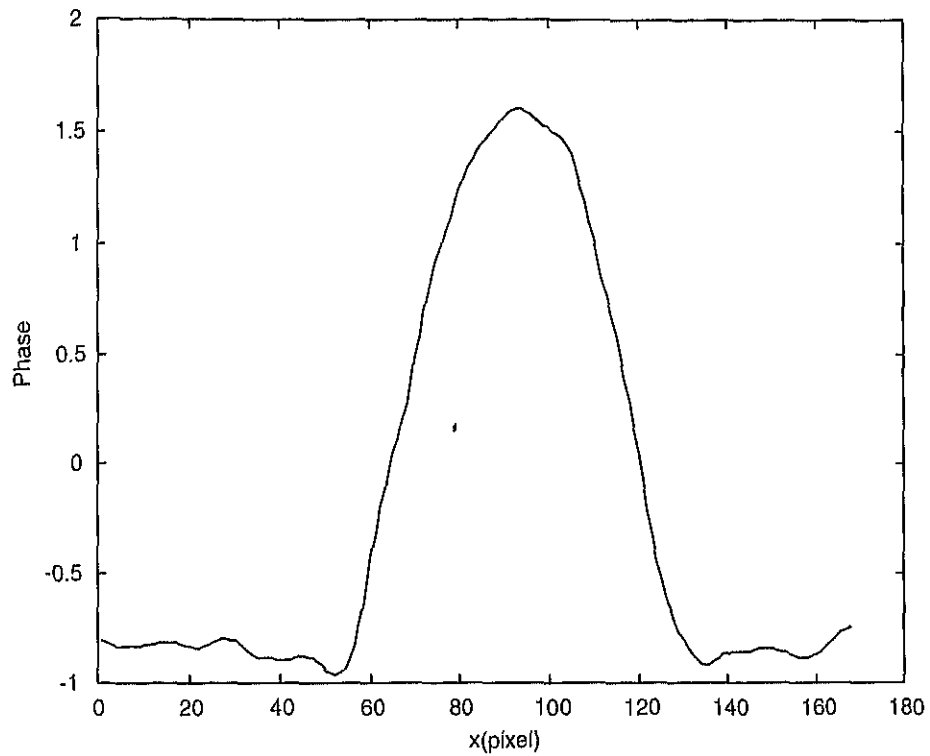


Fig. 10. The 1-D unwrapped phase profile of Fig. 9.

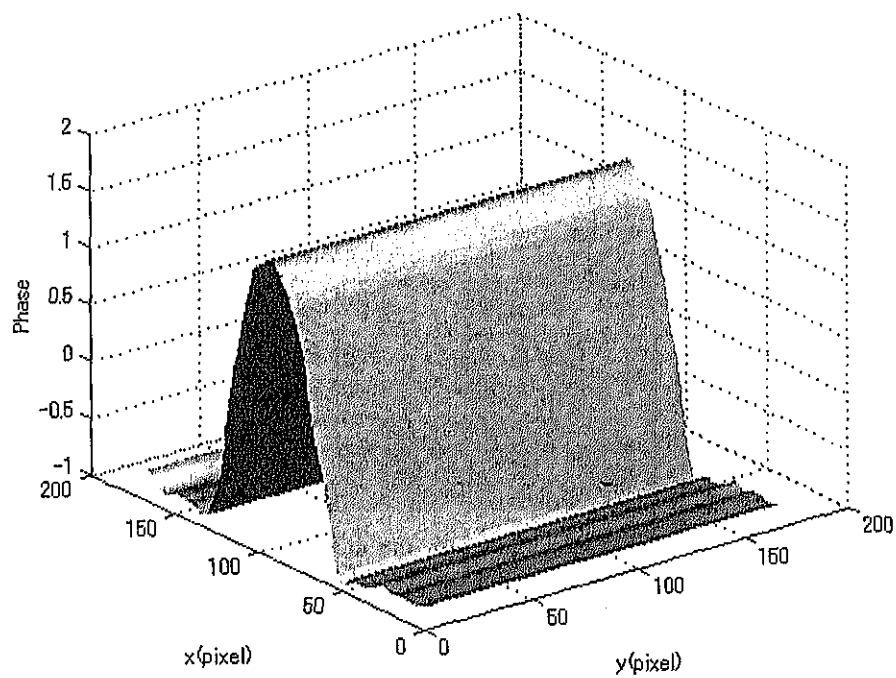


Fig. 11. Plot of the 2-D unwrapped continuous phase distribution of Fig. 9.

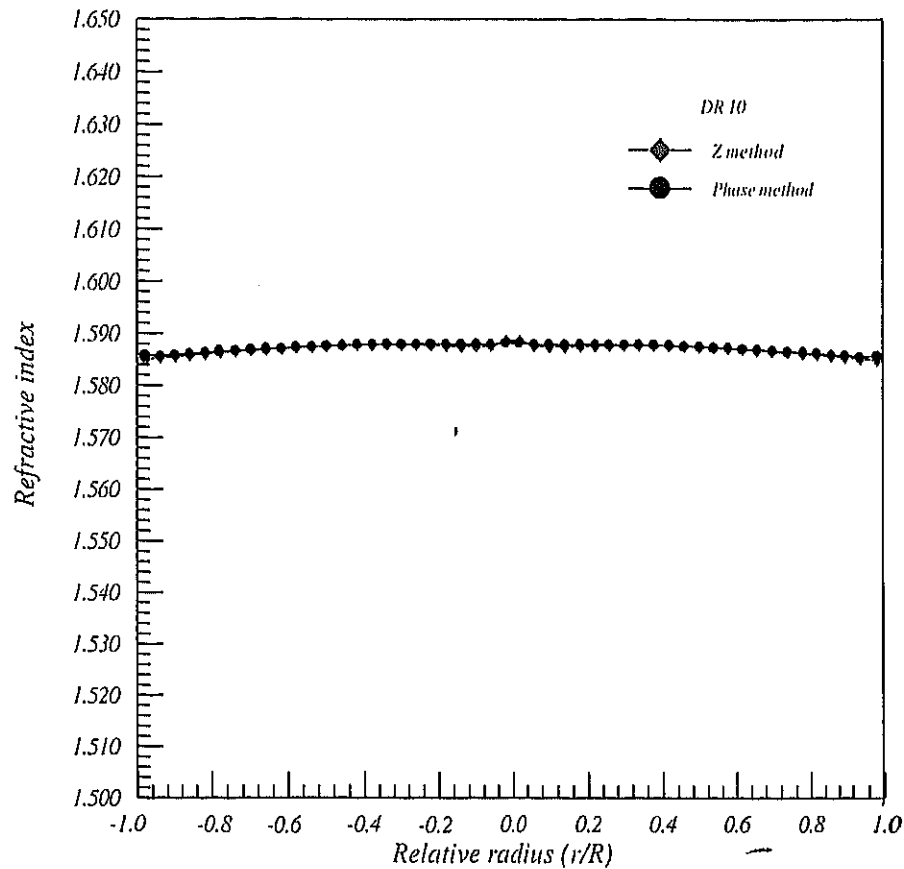


Fig. 12. Refractive index profile of polyethylene fiber with the draw ratio 10 using phase method and Z-method. Monochromatic light vibrating parallel to the fiber axis is used and the pixel size is found to be $0.625\mu\text{m}$ and the immersion liquid used is 1.5849.

Table 1

The Statistical comparisons between phase method and Z-method for the measured refractive index profile of polyethylene fiber having different draw ratios

Draw ratio	Pixel size (μ)	Standard deviation		Sigma error	
		Phase method	Fringe shift	Phase method	Fringe shift
7.5	1.317	9.560×10^{-4}	13.77×10^{-4}	9.331×10^{-7}	19.37×10^{-7}
7.5	0.867	8.781×10^{-4}	13.51×10^{-4}	7.871×10^{-7}	18.63×10^{-7}
10	0.625	8.016×10^{-4}	9.251×10^{-4}	6.560×10^{-7}	8.740×10^{-7}

5. Conclusions

The development of precise and efficient technique for refractive index profile measurement is an important technical task. Multiple-beam interference Fizeau

fringes system is applied to polyethylene fiber to determine its refractive index profile. FT method has been used for high-precision evaluation of the phase distribution of multiple-beam Fizeau fringes. By using Figs. 3 and 9, the measured radius of drawn polyethylene fibers 23.725 and 20.44 μm correspond to draw ratios 7.5 and 10, respectively. The refractive index profiles of drawn polyethylene fibers were obtained using the phase and fringe shift methods. We can conclude from the results that the phase method is a powerful technique to analyze the multiple-beam Fizeau fringes pattern and to measure the refractive index profile of fibers. Both the techniques perform equally well when applied to any interferogram having a low pixel size. The phase technique strategy presents two main benefits; (i) it is simple to automate and (ii) it performs better under certain circumstances, such as the case in high accuracy of refractive index profile measurement. Moreover, for large difference in fiber and immersion liquid refractive indices, it gives more stability of refractive index profile (see Table 1).

References

- [1] Zanger H, Zanger C. *Fibre optics communication and other applications*. New York: Macmillan, 1991.
- [2] Tolansky S. *Multiple-beam interferometry*. Oxford: Clarendon Press, 1948.
- [3] Barakat N, Hamza AA. *Interferometry of fibrous materials*. Bristol: Hilger, 1990.
- [4] Barakat N, Hamza AA, Gonied AS. Multiple-beam interference fringe applied to GR-IN optical waveguides to determine fibre characteristics. *Appl Opt* 1985;24:4383–6.
- [5] Hamza AA, Sokkar TZN, Mabrouk MA, Ghandar AM, Ramadan WA. On the determination of the refractive index of a fibre: II graded index fibre. *Pure Appl Opt* 1995;4:161–77.
- [6] Mabrouk MA, Shams-Eldin MA. Interferometric measurement of some structural parameters of drawn polyethylene fibres. *Pure Appl Opt* 1996;5:929–40.
- [7] Mabrouk MA, El-Bawab HF. Refractive index profile of GR-IN optical fibre considering the area under the interference fringe shift: I. The matching case. *Pure Appl Opt* 1997;6:247–56.
- [8] Yatagai T. Automated fringe analysis techniques in Japan. *Opt Laser Eng* 1991;15:79–91.
- [9] Morimoto Y, Fujisawa, Fringe pattern analysis by a phase-shifting method using Fourier transform. *Opt Eng* 1994;33:3709–14.
- [10] Hamza AA, Sokkar TZN, Mabrouk MA, El-Morsy MA. Refractive index profile of polyethylene fiber using interactive multiple-beam Fizeau fringe analysis. *J Appl Polym Sci* 2000;77:3099–106.
- [11] Bone DJ, Bachor HA, Sandemen RJ. Fringe-pattern analysis using a 2-D Fourier transform. *Appl Opt* 1986;25:1653–60.
- [12] Creath K. Phase measurement interferometry techniques. *Prog Opt* 1988;26:350–93.
- [13] Omura K, Yatagai T. Phase measuring Ronchi test. *Appl Opt* 1988;27(3):523–8.
- [14] Lai G, Yatagai T. Use of the fast Fourier transform method analyzing linear and equispaced Fizeau fringes. *Appl Opt* 1994;33(25):5935–40.
- [15] Nicola SD, Ferraro P. Fourier transform method of fringe analysis for Moire interferometry. *Pure Appl Opt* 2000;2:228–33.
- [16] Takeda M, Ina H, Kobayashi S. Fourier-transform method of fringe-pattern analysis for computer-based topography and interferometry. *J Opt Soc Am* 1982;72:156–60.
- [17] Takeda M, Mutoh K. Fourier transform profilometry for the automatic measurement of 3-D object shapes. *Appl Opt* 1983;22:3977–82.
- [18] Bruning HA. Fringe scanning interferometers. In: Malacara D, editor. *Optical shop testing*. New York: Wiley, 1978.

- [19] Green JR, Walker GJ, Robinson WD. Investigation of the Fourier-transform method of fringe pattern analysis. *Opt Laser Eng* 1988;8:29–44.
- [20] Liu BJ, Ronney DP. Modified Fourier transform method for interferogram fringe pattern analysis. *Appl Opt* 1997;36(25):6231–41.
- [21] Malacara D, Servin M, Malacara Z. *Interferogram analysis for optical testing*. New York: Marcel Dekker, 1998. p. 328–83.

Invited paper

Spatial light manipulation devices using nonlinear polymeric materials

K. HARADA¹, K. MUNAKATA¹, M. ITOH¹, S. UMEGAKI²
AND T. YATAGAI^{1,*}

¹*Tsukuba Advanced Research Alliance, Institute of Applied Physics, University of Tsukuba, 1-1-1 Tennodai, Tsukuba, Ibaraki 305-8573, Japan*

²*Faculty of Science and Engineering, Keio University, Hiyoshi, Yokohama 223-0061, Japan*

(*author for correspondence: E-mail: yatagai@bukko.bk.tsukuba.ac.jp)

Abstract. An electrically addressed spatial light modulator with 5×5 pixels is designed using nonlinear polymeric materials. Resonator structure for the material is proposed to minimize the driving voltages. Side-chain polymer poly-orange tom-1 isophoronedisocyanate ($r_{33} = 23$ pm/V) is used as a material. A modulation efficiency of 4.7% has been realized with 5.1 V_{rms} applied voltage at a wavelength of 633 nm. Very fast modulation at over 10 MHz has been demonstrated.

Key words: electrooptic effect, light modulator, organic material, polymeric material, resonator

1. Introduction

Spatial light modulators (SLMs) play very important roles for optical computing, such as optical neural network and optical image processing. Advances in SLM technologies therefore have a direct impact on these critical application. Liquid crystal SLMs generally used in optical computing have a very slow modulation speed and a low contrast ratio. Ferroelectric liquid crystal SLMs have a high modulation speed, but the modulation speed is <100 kHz. Because the mechanism (reorientation of molecules when applied voltage) limits the response time of the devices, faster modulation speed can not be expected by using liquid crystal SLMs. Development of sophisticated SLMs with very fast modulation speed is essential. Multiple-quantum-well (MQW) smart pixels are one of the most promising high speed SLMs, but there are limitations on device size and spatial resolution. Another candidate for SLM material is an amorphous nonlinear polymer. These are very attractive for electro-optical applications as they have a low and nearly non-dispersive dielectric function. Their fabrication is easy compared with growing single crystals of organic and inorganic materials. The dielectric constants of polymeric materials are about 3, which is 1/10 of LiNbO₃. Low dielectric constant makes it possible to operate polymer devices at very high

frequency. Operation at 40 GHz was demonstrated with poled polymer optical modulator (Teng 1992). In recent years, considerable progress has been made in the development of nonlinear organic materials having large nonlinearities and thermal stability. A maleimide-based copolymer, PMPD (Kato *et al.* 1998) is one of the most promising materials, and it was demonstrated that this polymer had a large optical nonlinearity, a long-term stability and a fast modulation speed. The measured electro-optic coefficient is twice as large as that of LiNbO₃. This electro-optic coefficient is sufficient for a waveguide light modulator to control the light, but is insufficient for a SLM because the effective pass length is much shorter than that of a waveguide light modulator. The problem can be solved using Fabry–Perot etalons because they increase the effective optical path length acting across the spacer region, and minimize the drive voltages (Harada *et al.* 1996).

We will discuss here the advantages of these polymeric materials and the development of SLMs using them. We have simulated and demonstrated the electrically induced changes in light intensity using polymeric thin film in a Fabry–Perot structure.

2. Simulation of light modulation using resonator structure

We simulated the light modulation of the polymeric Fabry–Perot etalons. A film poled in the direction of the surface normal has the electrooptic tensor expressed as:

$$\begin{pmatrix} 0 & 0 & r_{13} \\ 0 & 0 & r_{13} \\ 0 & 0 & r_{33} \\ 0 & r_{13} & 0 \\ r_{13} & 0 & 0 \\ 0 & 0 & 0 \end{pmatrix},$$

where $r_{33} = 3r_{13}$ (Singer *et al.* 1986).

For an electric field in the direction of the surface normal (z-direction), the equation for the refractive index ellipsoid is

$$\left(\frac{1}{n_o^2} + r_{13}E_z\right)(X^2 + Y^2) + \left(\frac{1}{n_e^2} + r_{33}E_z\right)Z^2 = 0, \quad (1)$$

where X , Y , and Z refer to the laboratory axes parallel to the principal dielectric axes parallel to the principal dielectric axes of the film, and n_o and n_e are the ordinary and extraordinary refractive indices respectively. On

application of an electric field in the direction of surface normal, the change in refractive index experienced by ordinary ray is thus,

$$\Delta n_o = -\frac{1}{2}n_o^3 r_{13} E_z \quad (2)$$

and for the extraordinary rays,

$$\Delta n_e = -\frac{1}{2}n_e^3 r_{33} E_z. \quad (3)$$

Changes in the indices of refraction experienced by the ordinary ray can be related to the modulation voltage V by the expressions, using Equation (2) as

$$\Delta n_o = -\frac{1}{2}n_o^3 r_{13} \frac{V}{l}, \quad (4)$$

where l is the separation between the two indium tin oxide (ITO) electrodes. This induced Δn_o changes the device transfer characteristics by the phase change in the polymeric layer. The use of a resonator structure is proposed to minimize the driving voltages.

Fig. 1 shows the device structure. A polymer film was sandwiched between dielectric mirrors. Quarter-wave stacks of dielectric material is arranged in such way that alternating layers have a low index of reflection $n_1 = 1.46$ (SiO_2) and high index of reflection $n_2 = 2.35$ (TiO_2). The thickness of each layer is $\lambda/4n_1$, $\lambda/4n_2$, where λ is the free-space wavelength (633 nm).

Transmission spectrum can be calculated theoretically by solving the boundary condition of each layers. The device shows a sharp spectrum in a specific wavelength determined by the polymer film thickness and refractive index. Fig. 2 shows the calculated transmission spectrum when each dielectric mirror is 10 layers and the optical thickness of the polymer is $\lambda/2$, where λ is the free-space wavelength (633 nm). In this simulation, there is no optical loss of the sample. We can control the intensity of monochromatic light by changing the refractive index of the polymer by applying an electric field. Fig. 3 shows the applied voltage dependence of transmission spectrum around 633 nm when each dielectric mirror is 10 layers and electro-optic

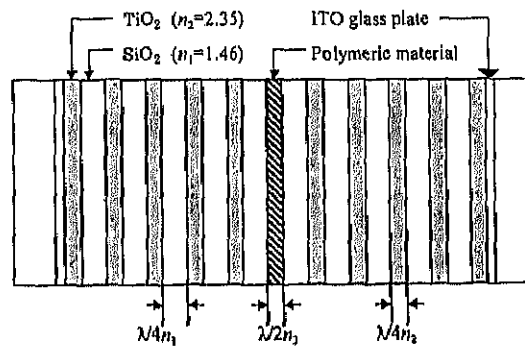


Fig. 1. Resonator structure for polymeric materials.

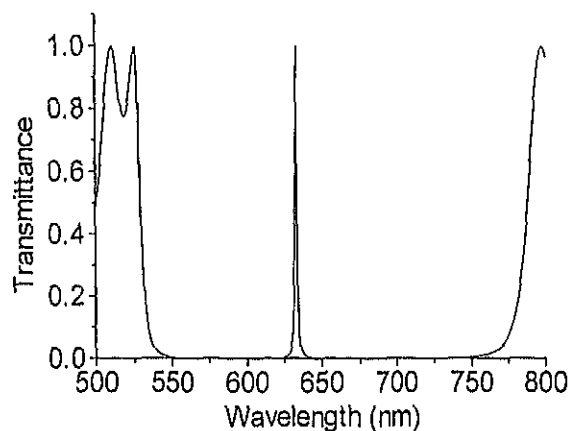


Fig. 2. Calculated transmission spectrum when each dielectric mirror is 10 layers.

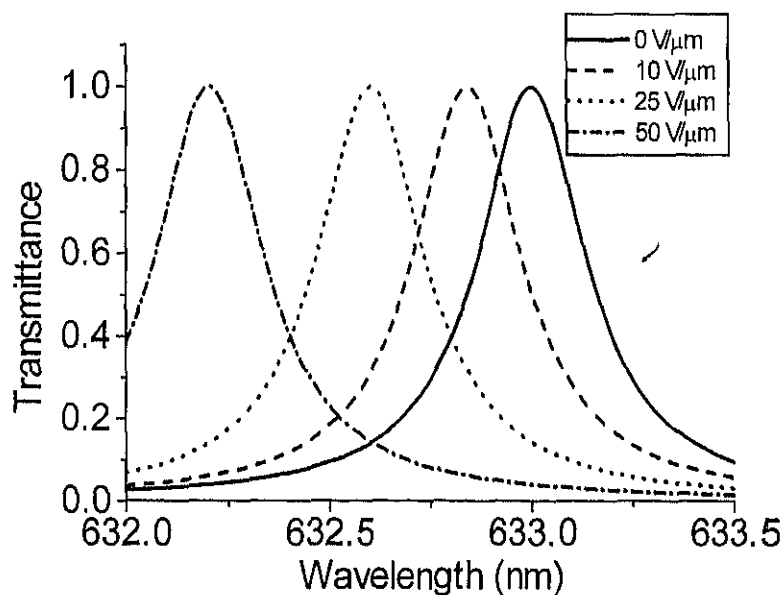


Fig. 3. Applied voltage dependence of transmission spectrum when each dielectric mirror is 10 layers and electro-optic coefficient is 20 pm/V.

coefficient is 20 pm/V. Transmission peak shifts by applying electric field. The contrast ratio of 10 layered sample in this case is estimated as about 40:1 when the applied voltage is 50 V/μm.

3. Polymeric spatial light modulator with 5×5 pixels

Polymeric SLM with 5×5 pixels is designed. Side-chain polymer poly-orange tom-1 isophoronedisocyanate (Itoh *et al.* 1998) is used as a polymeric material in this study. Fig. 4 show the chemical structure of poly-orange tom-1 isophoronedisocyanate. Absorption spectrum of the material is shown in Fig. 5. Cutoff wavelength of the material is about 600 nm and it is trans-

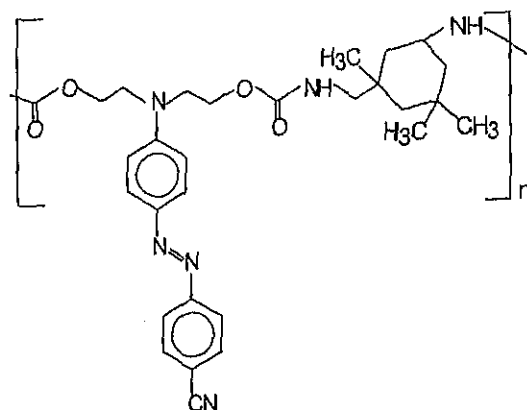


Fig. 4. Chemical structure of poly-orange tom-1 isophoronedisocyanate.

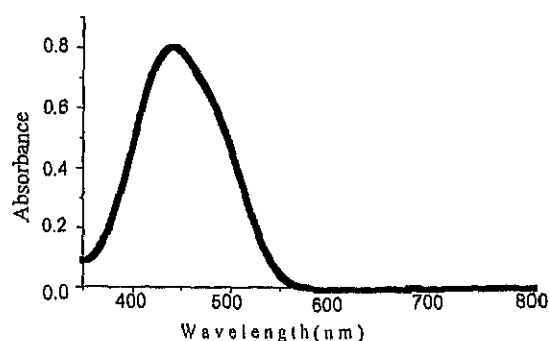


Fig. 5. Absorption spectrum of poly-orange tom-1 isophoronedisocyanate.

parent at 633 nm. The glass transition temperature T_g is 136°C. The refractive index is 1.7 at a wavelength of 633 nm. The electrooptic coefficient r_{33} is measured by a reflection technique (Teng and Man 1990).

The measured electrooptic coefficient r_{33} is 23 pm/V at the wavelength of 633 nm. Half-wave voltage of the device using this material is estimated about 20 kV. The use of a resonator structure is proposed to minimize the driving voltages. The polymer dissolved in cyclohexanone is spin-coated on the glass plate with multilayered dielectric mirror and ITO electrode. Then another multilayered dielectric mirrors and ITO electrode are coated on the polymer film. Photo assisted poling was performed to align the chromophore orientation with an applied voltage of 100 V across the polymer film for 20 min by irradiating Ar^+ laser. There are simple matrices with 25 pixels and the size of one pixel is 1×1 mm. Each mirror is composed of 12 layers. The reflectivity of the dielectric mirror is about 95% at the wavelength of 633 nm.

By using a spectrometer (Jasco Co., V-530), we measured the transmittance characteristics of the device when the incident light was normal to the sample (Fig. 6). The device shows a sharp spectrum at 590 and 680 nm. He-Ne laser (633 nm) is used in this experiment. There is no transmission peak at 633 nm. Maximum modulation efficiency is expected by choosing the transmission peak at the experimental wavelength. By changing

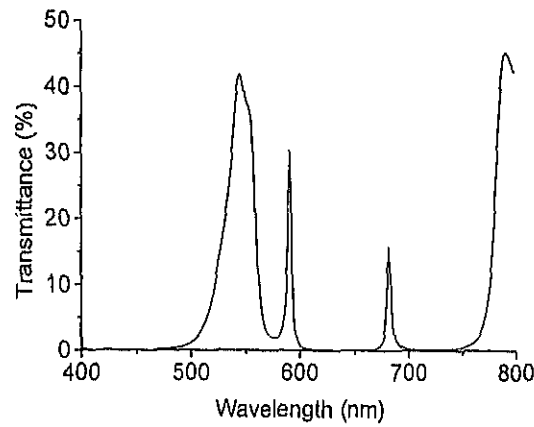


Fig. 6. Transmittance characteristics of the device.

the input angle, we can adjust the transmission peak at proper wavelength. Fig. 7 shows the angler dependence of the transmission intensity at the wavelength of 633 nm. The transmittance increases near 47° . The maximum transmittance of 20% is obtained at the incident angle of 47° .

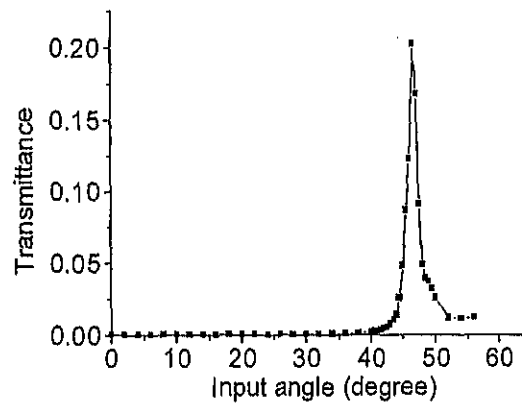


Fig. 7. Angler dependence of the transmission intensity at the wavelength of 633 nm.

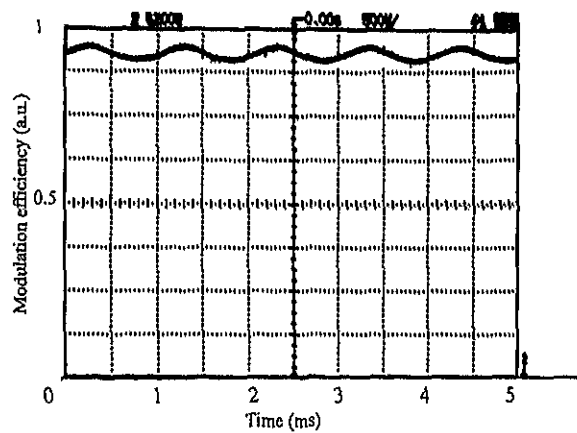


Fig. 8. Light modulation of the laser beam. Current voltage of 1 kHz with 5.1 V_{rms} is applied.

Fig. 8 shows the results of the light modulation at the input angle of 47° . Operation at 10 MHz is demonstrated with each pixels, and modulation efficiency of 4.7% is obtained at 1 kHz with 5.1 V_{rms} applied voltage. A maximum modulation efficiency of 18.8% is obtained at an applied voltage of 34 V_{rms}.

4. Conclusion

Electrically addressed SLMs with 5×5 pixels is designed using poled polymer. The use of a resonator structure is proposed to minimize the driving voltage. Side-chain polymer poly-orange tom-1 isophoronedisocyanate ($r_{33} = 23$ pm/V) is used as a material. Operation at 10 MHz is demonstrated with each pixels, and modulation efficiency of 4.7% is obtained at 1 kHz with 5.1 V_{rms} applied voltage. We have already reported the light modulation on Si integrated circuits (Harada *et al.* 1998). These etalon modulators with polymeric materials have applications in optical computing, including of optical neural networks and optical image processing.

Acknowledgements

We wish to thank Hamamatsu Photonics Co. for making multilayered dielectric mirrors. This research was partly supported by a Grant-in-Aid for Scientific Research from the Ministry of Education, Science, Sports and Culture and by the Yatagai Project, Tsukuba Advanced Research Alliance, University of Tsukuba.

References

- Harada, K., M. Itoh and T. Yatagai. *Opt. Rev.* **3** 440, 1996.
- Harada, K., H. Munakata, M. Itoh, N. Yoshikawa, H. Yonezu, S. Umegaki and T. Yatagai. *Jpn. J. Appl. Phys.* **37** 4393, 1998.
- Itoh, M., K. Harada, H. Matsuda, S. Ohnishi, A. Parfenov, N. Tamaoki and T. Yatagai. *J. Phys. D: Appl. Phys.* **31** 463, 1998.
- Kato, M., T. Shiraga, T. Fukuda, H. Matsuda and H. Nakanishi. *J. Photopolym. Sci. Technol.* **11** 161, 1998.
- Singer, K.D., J.E. Sohn and S.J. Lalama. *Appl. Phys. Lett.* **49** 248, 1986.
- Teng, C.C., *Appl. Phys. Lett.* **60** 1538, 1992.
- Teng, C.C. and H.T. Man. *Appl. Phys. Lett.* **56** 1734, 1990.